WILL Relational Geometry

Relational Approach to Dark Sector Problem in Cosmology

Anton Rize
antonrize@willrg.com

January 2026

Abstract

In this work, we apply the principles of WILL Relational Geometry (RG) to the domain of cosmology and galactic dynamics. By strictly enforcing geometric closure conditions with **zero free parameters**, we establish a sequential unbroken chain of derivations from first principles to observational evidence.

1. **Hubble parameter:** we derive ($H_0 \approx 68.15$ km/s/Mpc) solely from the CMB temperature and the fine-structure constant (α) providing the direct bridge between scales and landing within 1% of Planck 2018 mission measurement ($H_0 \approx 67.4$ km/s/Mpc).
2. **Distant Supernova Flux Levels:** using this H_0 value along with kinetic and potential geometric weights we compare the curve with **Pantheon+** dataset - deviations remains below 0.015 mag across the entire redshift range.
3. **CMB Acoustic Spectrum:** utilizing same derived horizon scale, we reconstruct the CMB acoustic spectrum as the resonant harmonics of an S^2 topology loaded by $\approx 4.2\%$ baryons, naturally resolving the "Low Quadrupole" anomaly via vacuum tension.
4. **Galactic Rotation Curves:** we translate the global horizon into a local acceleration scale ($a_\kappa = cH_0/3\pi$), which we apply to the SPARC database (175 galaxies). This rigid geometric prescription predicts rotation curves, the Radial Acceleration Relation (RAR), and the linear scaling of Phantom Inertia with equal or higher precision than MOND phenomenology, without any fitting.
5. **Dark Lensing:** we extend this framework to the gravitational lensing of "dark" potentials showing that the same Phantom Inertia responsible for galactic dynamics, also stands behind the "dark lensing" phenomena.
6. **Wide Binary Stars:** applied to this dynamic systems the theory correctly predicts the kinetic resonance scale ($a_\beta = cH_0/6\pi$) matching recent Gaia DR3 within observational uncertainties.

These results show that the framework reproduces the considered empirical constraints across approximately 20 orders of magnitude. Taken together, these results *motivate* considering a **relational-geometric ontology** as a viable alternative to dark-sector phenomenology, and they *warrant further* empirical stress-testing across independent datasets.

 DOI: 10.5281/zenodo.17115270

Contents

1 Methodological Framework (WILL RG Part I Recap)

1.1 Ontological Principle: Generative Physics (Results Established in WILL RG Part I)

Standard cosmological models operate on a descriptive paradigm, fitting dynamical laws (Lagrangians) onto a pre-existing spacetime manifold. We adopt a strictly **generative** approach based on the foundational principle established in WILL Relational Geometry (Part I):

$$\boxed{\text{SPACETIME} \equiv \text{ENERGY}}$$

Throughout this paper, the identity is to be read as an ontological identification,

not as an algebraic equation or a dynamical law.

This principle asserts that "spacetime" and "energy" are not distinct entities but dual projections of a single invariant relational structure. Consequently, we do not postulate a background metric. Instead, geometry emerges solely from the conservation requirements of closed relational carriers.

1.2 The Relational Carriers: S^1 and S^2

The topology of a closed, maximally symmetric system admits exactly two minimal relational carriers for the energy budget:

1. **Kinematic Carrier (S^1):** Encodes directional transformation (1 Degree of Freedom). Its state is defined by the orthogonal projections:

   $$\beta^2 + \beta_Y^2 = 1$$

   where $\beta = v/c$ is the kinematic amplitude (external motion) and $\beta_Y = 1/\gamma$ is the phase (internal time rate).

2. **Potential Carrier (S^2):** Encodes omnidirectional interaction (2 Degrees of Freedom). Its state is defined by:

   $$\kappa^2 + \kappa_X^2 = 1$$

   where $\kappa^2 = R_s/r$ represents the gravitational potential intensity and κ_X is the structural phase (gravitational redshift).

(z = gravitational redshift) (z_D = transverse Doppler shift)

 DOI: 10.5281/zenodo.17115270

$\theta_1 = \arccos(\beta), \quad \theta_2 = \arcsin(\kappa), \; \kappa^2 = 2\beta^2$	
Algebraic Form	**Trigonometric Form**
$\beta = v/c = \sqrt{1 - \frac{1}{(1+z_D)^2}}$	$\beta = cos(\theta_1)$
$\kappa = \sqrt{R_s/r} = \sqrt{1 - \frac{1}{(1+z)^2}}$	$\kappa = sin(\theta_2)$
$\beta_Y = \sqrt{1-\beta^2}$	$\beta_Y = \sin(\theta_1) = \sin(\arccos(\beta))$
$\kappa_X = \sqrt{1-\kappa^2}$	$\kappa_X = \cos(\theta_2) = \cos(\arcsin(\kappa))$
$p = E_0/c \cdot \beta/\beta_Y$	$p = E_0/c \cdot \cot(\theta_1)$
$p_g = E_0/c \cdot \kappa/\kappa_X$	$p_g = E_0/c \cdot \tan(\theta_2)$
$\tau = \beta_Y \kappa_X$	$\tau = \sin(\theta_1)\cos(\theta_2)$
$Q = \sqrt{\kappa^2 + \beta^2} = \sqrt{3}\beta$	$Q = \sqrt{3}\cos(\theta_1)$

Table 1: Unified representation of relativistic and gravitational effects for closed systems.

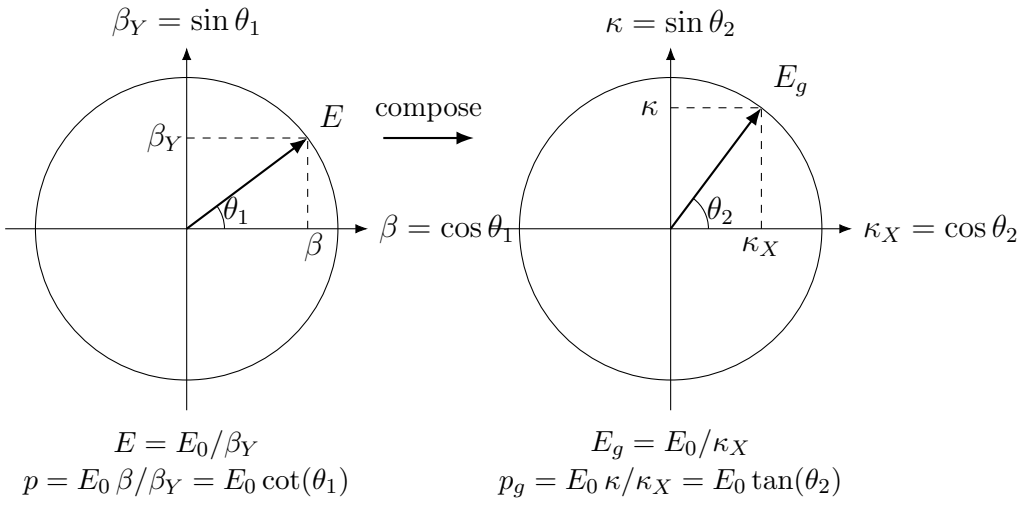

1.3 The Energetic Closure Condition

For any stable, self-contained system, the energy budget must be partitioned between these carriers. The exchange rate is strictly determined by the ratio of their relational degrees of freedom ($\mathrm{DOF}_{S^2}/\mathrm{DOF}_{S^1} = 2$). This yields the fundamental **Closure Condition** governing all bound systems (virial equilibrium):

$$\boxed{\kappa^2 = 2\beta^2}$$

This geometric identity replaces the Newtonian dynamical postulate. It implies that for any closed system, the gravitational potential energy (κ^2) must be exactly twice the kinetic energy (β^2) to maintain topological stability.

1.4 Total Relational Shift and Self-Centering Reciprocity

Interaction between observers is defined by the **Total Relational Shift** (Q), which measures the magnitude of displacement from the observer's origin on a (β, κ) plane (1):

$$Q^2 = \beta^2 + \kappa^2 \tag{1}$$

Under the closure condition (1.3), this norm simplifies to $Q^2 = 3\beta^2 = \frac{3}{2}\kappa^2$.

The **Potential Relational Weight** of the total shift is: $\Omega_{pot} = \frac{\kappa^2}{Q^2} = \frac{2}{3}$. The **Kinematic Relational Weight** of the total shift is: $\Omega_{kin} = \frac{\beta^2}{Q^2} = \frac{1}{3}$.

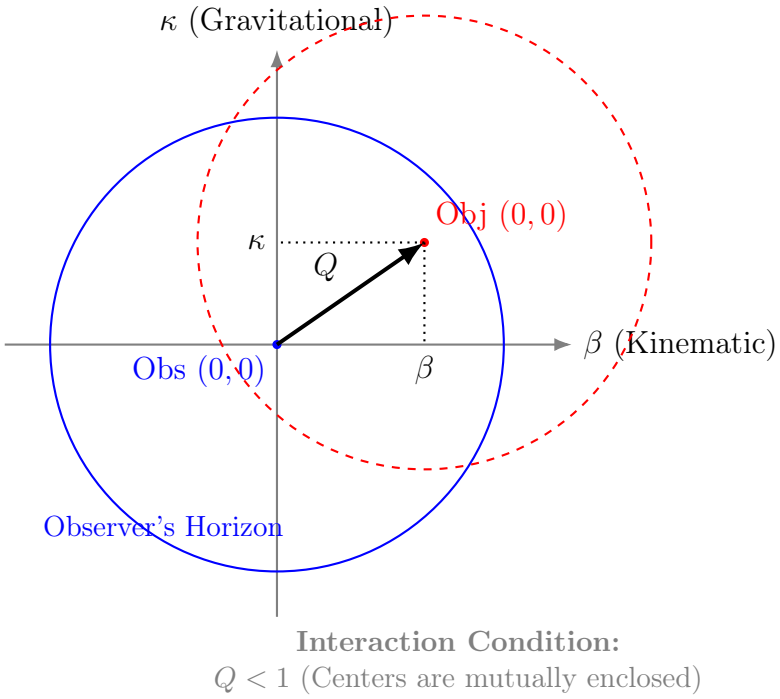

Figure 1: **Relational Self-Centering.** The relational shift Q is defined by the orthogonal projections β and κ. Interaction is causal only when the center of the Object lies within the Observer's horizon ($Q < 1$), ensuring mutual coverage.

2 The Necessity of Global Resonance

Remark 2.1. *Throughout this document, the word Universe means the relational system within the observer's causal boundaries.*

Having established that the relational carriers of WILL are topologically closed (WILL Part I: Lemma Closure), we now derive the consequences of closure for persistent dynamics. Consequently, since SPACETIME ≡ ENERGY, any spatial separation is defined intrinsically by relational energy differentials.

Lemma 2.2 (Inevitability of Self-Interaction)**.** *In a closed relational carrier $\mathcal{C}$ with finite measure, any relational perturbation cannot propagate indefinitely without re-encountering its own wavefront.*

Proof. Since $\mathcal{C}$ is compact and boundary-free (WILL RG Part I: Lemma Closure), any causal propagation along $\mathcal{C}$ is recurrent. Therefore the local relational state generically includes contributions from its own propagated history (echoes). □

Theorem 2.3 (Global Phase-Closure Constraint)**.** *Persistent modes on a closed relational carrier must satisfy global phase closure. Modes incompatible with closure do not accumulate Total Relational Shift (Q_{total}) under repeated self-interaction.*

Proof. By Lemma 2.2, strictly closed topology necessitates recurrent propagation. Let the relational state be represented by a shift vector $\vec{Q}$ with phase angle ϕ. According to the Precession Law, each full cycle on the carrier induces a phase shift $\Delta_\phi \propto Q^2$.

The Total Relational Shift of the mode is determined by the coherent vector sum of its history (superposition). We compare two cases:

1. **Resonance ($\Delta_\phi = 2\pi n$):** The phase shift is a full rotation. The shift vectors $\vec{Q}$ of each subsequent cycle are collinear. The magnitude of the total shift $Q_{total} = ||\sum \vec{Q}_i||$ grows linearly with the number of cycles (N). Since SPACETIME $\equiv$ ENERGY and Energy $\propto Q^2$, this accumulation allows the mode to reach the saturation limit required for a persistent physical manifold.

2. **Dissonance ($\Delta_\phi \neq 2\pi n$):** The shift vectors of subsequent cycles are misaligned by angle Δ_ϕ. Geometrically, their vector sum traces a bounded trajectory whose net magnitude does not grow with N. The total shift magnitude Q_{total} does not grow with N but remains trapped within a finite, microscopic limit ($Q_{total} \ll 1$).

Conclusion: In a generative ontology, only resonant modes can accumulate sufficient Relational Shift Q to form the macroscopic "Fundamental Tone" of the Universe. All non-resonant modes are self-canceling fluctuations that fail to manifest as spacetime structure. □

This implies that a single mode oscillation corresponds to the Fundamental Tone of the observable Universe. Our methodology strictly precludes the acceptance of empirically fitted values (like H_0); instead, we must derive it from first principles. To find this exact Tone, we rely on the core principle of WILL RG:

$$\boxed{\text{SPACETIME} \equiv \text{ENERGY}}$$

3 Deriving H_0 from CMB Temperature and α

The most robust, model-independent absolute scale available in cosmology is the monopole temperature of the Cosmic Microwave Background (T_0). It defines the current radiation energy density ρ_γ.

As derived in WILL RG Part III, the fine-structure constant α acts as the kinematic projection of the ground state ($\beta_1 \equiv \alpha$), connecting micro- and macro-closure. This fixes the RG scaling ratio between the radiation density ρ_γ and the geometric saturation density ρ_{max} (derived in WILL Part I as density at $r = R_s \implies \kappa^2 = 1$).

3.1 Prerequisite: The Geometric Identity of α (Summary of Part III)

In WILL RG III (click to see derivation) atomic stability is derived not from force equilibrium, but from the **Geometric Closure Condition** between the potential (S^2) and kinetic (S^1) carriers: $\kappa^2 = 2\beta^2$.

We defined the **Electromagnetic Critical Radius** (R_q) as the scale of energetic saturation ($U = E_{rest}/2$), and the **Bohr Radius** (a_0) as the scale of topological phase closure ($n = 1$). The Fine Structure Constant α is rigorously identified as the unique

Kinematic Projection (β_1) required to bridge these two scales: Derived in WILL RG III (click to see derivation)

$$\alpha \equiv \beta_1 = \sqrt{\frac{1}{2}\frac{R_q}{a_0}} \tag{2}$$

Thus, α is the scaling factor defining the ratio between the **critical limit of the field** and the **stable state of matter**. This rigid geometric scaling ($\beta \leftrightarrow \kappa$) allows us to use α to map the macroscopic saturation density ρ_{max} in the following section.

3.2 Input Parameters and Constants

All input values are taken from standard CODATA (2018) and Planck (2018) datasets. No model-specific fitting parameters are used.

Parameter	Symbol	Value	Source/Definition
CMB Temperature	T_0	2.7255	Fixsen (2009) / Planck
Fine Structure Const.	α	7.29735e-3	CODATA ($\approx 1/137.036$)
Gravitational Const.	G	6.674e-11	CODATA
Speed of Light	c	2.99792e8	Exact
Stefan-Boltzmann Const.	σ_{SB}	5.67037e-84	Derived from fundamental constants height

Table 2: Core inputs for the calculation. Colab notebook link: H_0 from T_{CMB} and α.ipynb

3.3 Step-by-Step Derivation

3.4 Step 1: Radiation Density Calculation (ρ_γ)

Objective: Determine the photon mass-energy density of the Universe. This provides the "Energy" input for the $Spacetime \equiv Energy$ equivalence.

$$\rho_\gamma = \frac{4\sigma_{SB}T_0^4}{c^3} \tag{3}$$

Using the input $T_0 = 2.7255$ K:

$$\rho_\gamma \approx 4.641 \times 10^{-31}\,\mathrm{kg/m^3} \tag{4}$$

3.5 Step 2: Maximal Structural Density (ρ_{max})

Objective: Calculate the saturation structural density of the system.

Lemma 3.1 (Dynamical Normalization)**.** *In the Normalization Identity (derived in WILL RG I), the ratio $\kappa^2 = \rho/\rho_{max}$ was derived for a static gravitational configuration, where the energy resides entirely in the potential carrier (S^2). We now extend this to a dynamical, energy-closed system where both carriers are active.*

In WILL RG, the saturation density $\rho_{max}(r) = c^2/(8\pi G r^2)$ is a property of the geometric manifold at scale r. It represents the maximal energy capacity per unit carrier projection:

- *For the potential carrier (S^2): $\kappa^2 = \rho_{pot}/\rho_{max}$, as established.*

 DOI: 10.5281/zenodo.17115270

- *For the kinetic carrier (S^1): $\beta^2 = \rho_{kin}/\rho_{max}$, by the same geometric construction - the kinetic projection β^2 measures the fraction of the systems capacity occupied by kinetic energy.*

Both projections are normalized against the same ρ_{max} because the saturation density is a property of the geometry itself (the capacity of the system at scale r), not of the energy configuration projected onto it. This is a direct consequence of the ontological identity principal SPACETIME ≡ ENERGY: there is one system, and both carriers project onto it.

Therefore, the total energy density of a closed dynamical system, expressed as a fraction of the geometric capacity, is given by the full Relational Shift:

$$\boxed{Q^2 = \kappa^2 + \beta^2 = \frac{\rho_{total}}{\rho_{max}}} \tag{5}$$

Verification. At the Global Horizon ($r = c/H_0$), the closure condition at saturation gives $\beta^2 = 1$ and $\kappa^2 = 2$. The corresponding densities are:

$$\rho_\beta = \beta^2 \cdot \rho_{max} = 1 \times \frac{c^2}{8\pi G r^2} \approx 2.908 \times 10^{-27}\,\mathrm{kg/m^3}, \tag{6}$$

$$\rho_\kappa = \kappa^2 \cdot \rho_{max} = 2 \times \frac{c^2}{8\pi G r^2} \approx 5.815 \times 10^{-27}\,\mathrm{kg/m^3}. \tag{7}$$

Their sum yields:

$$\rho_\beta + \rho_\kappa = 3\rho_{max} = Q^2 \rho_{max}, \tag{8}$$

confirming the identity $Q^2 = (\rho_\beta + \rho_\kappa)/\rho_{max} = 3$ at the horizon, consistent with $\kappa^2 + \beta^2 = 2 + 1 = 3$. □

3.5.1 Application to the Electromagnetic Ground State

The geometric identity $\alpha \equiv \beta_1$ (derived in WILL RG III) defines the kinematic projection of the electromagnetic vacuum. Combined with the Closure Condition ($\kappa^2 = 2\beta^2$), this fixes both carrier projections of the EM ground state:

$$\beta^2_{EM} = \alpha^2, \qquad \kappa^2_{EM} = 2\alpha^2. \tag{9}$$

Since the photon field is a dynamical, energy-closed configuration - not a static potential - its total energy density occupies both carriers simultaneously. Applying the Dynamical Normalization (Lemma 3.1):

$$\frac{\rho_\gamma}{\rho_{max}} = Q^2_{EM} = \kappa^2_{EM} + \beta^2_{EM} = 2\alpha^2 + \alpha^2 = 3\alpha^2 \tag{10}$$

Rearranging for ρ_{max}:

$$\boxed{\rho_{max} = \frac{\rho_\gamma}{3\alpha^2}} \tag{11}$$

Using $\alpha \approx 7.297 \times 10^{-3}$ (where $\alpha^2 \approx 5.325 \times 10^{-5}$):

$$\rho_{max} \approx \frac{4.645 \times 10^{-31}}{3 \cdot 5.325 \times 10^{-5}} \approx 2.908 \times 10^{-27}\,\mathrm{kg/m^3} \tag{12}$$

This value is in precise agreement with cosmological expectations ($\rho_{crit} \approx 9.5 \times 10^{-27}$ kg/m^3; $\rho_{max} \approx \rho_{crit}/3$), providing a Machian connection between the microphysical constant α and the macroscopic geometry.

3.6 Step 3: The Hubble Parameter (H_0)

Objective: Convert the saturation density into the frequency parameter.

Logic: Using the WILL RG saturation identity $\rho_{max}(r) = c^2/(8\pi G r^2)$ together with the horizon definition $H_0 = c/r$, we obtain the relation:

$$H_0 = \sqrt{8\pi G \rho_{max}}. \tag{13}$$

3.7 Results and Numerical Calculation

Substituting the derived ρ_{max} into the final equation:

$$\begin{aligned} H_0 &= \sqrt{8\pi \cdot (6.674 \times 10^{-11}) \cdot (2.907 \times 10^{-27})} \\ H_0 &= \sqrt{4.877 \times 10^{-36}} \\ H_0 &\approx 2.2084503668 \times 10^{-18}\,\mathrm{s}^{-1} \end{aligned}$$

3.8 Unit Conversion

Converting from SI units (s^{-1}) to standard cosmological units (km/s/Mpc):

$$\text{Conversion Factor} = \frac{3.0857 \times 10^{22}\ \text{m/Mpc}}{1000\ \text{m/km}} \approx 3.0857 \times 10^{19}$$

$$H_0 \approx 2.208 \times 10^{-18} \times 3.0857 \times 10^{19} \approx \mathbf{68.15}\,\text{km/s/Mpc} \tag{14}$$

Remark 3.2 (Metric Selectivity and Neutrino Exclusion)**.** *Standard cosmological models (e.g., ΛCDM) aggregate all relativistic species (photons + neutrinos) into a single radiation density term ρ_{rad}, assuming universal gravitational coupling via the stress-energy tensor.*

WILL RG Distinction: *In a relational ontology, the metric extension of spacetime is defined by the specific interaction carrier.*

1. *The Observable Horizon H_0 constitutes the limit of* ***Electromagnetic Causality*** *(defined by c).*
2. *The geometric scaling of this horizon is governed by the* ***Electromagnetic Coupling*** *α (derived in Part III).*
3. *Neutrinos interact exclusively via the Weak Force and gravity; they do not couple to the electromagnetic carrier $S^1(\alpha)$.*

Therefore, including the neutrino background (ρ_ν) in the definition of an α-governed horizon would constitute a category error. The geometric saturation ρ_{max} is normalized strictly against the energy density of the carrier field defining the metric - the photon "gas" ρ_γ.

 DOI: 10.5281/zenodo.17115270

3.9 Discussion of the Cosmological Anchor

The calculated value $H_0 \approx 68.15$ km/s/Mpc is derived without any free parameters or model fitting. It relies exclusively on the measured CMB temperature and the identification of the fine-structure constant α as the geometric scaling of the ground state.

- **Comparison with Planck (2018):** The Planck result is 67.4 ± 0.5 km/s/Mpc. Our result deviates by approximately $+1.0\%$.
- **Comparison with SH0ES (2019):** The local ladder measurement is 74.0 ± 1.4 km/s/Mpc. Our result supports the "Early Universe" (CMB) measurements.
- **Methodological Implication:** The high precision of this result suggests that the "Hubble Tension" may not be a crisis of measurement, but a confirmation that the Universe operates as a geometrically closed system where micro-constants (α) and macro-parameters (H_0) are rigidly locked.

Result: WILL Relational Geometry successfully bridges Quantum Mechanics (WILL RG Part III) and Cosmology (WILL RG Part I and II), yielding a theoretically grounded value for H_0 that matches observations.

4 Phase Evolution and the Geometric Origin of the CMB

In the WILL Relational Geometry framework, the history of the Universe is not measured by absolute Newtonian time, but by the accumulation of relational phase, o. Having established the Universal Horizon scale (H_0) and the kinematic projection of the ground state (α), we now derive the epoch of "First Light" (Recombination) as a necessary geometric transition, rather than a thermodynamic accident.

4.1 The Mechanism of Expansion: Cumulative Phase Divergence

In WILL RG I (Section 16.5), we derived the universal precession law for any bound relational system. This law describes the irreducible phase shift (angular defect) accumulated over one orbital cycle due to the system's total relational energy shift Q^2.

$$\Delta_\phi = \frac{2\pi Q^2}{1 - e^2} \tag{15}$$

To describe the global evolution of the Universe, we apply this law to the **Cosmological Ground State**. This state is defined by three strict geometric conditions enforced by the Principle of Isotropy and the Part III derivation of atomic stability:

1. **Global Isotropy (Circular Limit):** The vacuum state of the Universe is maximally symmetric, implying zero eccentricity.
$$e \to 0$$
2. **Ground State Coupling:** The kinematic projection of the vacuum is defined by the fine-structure constant α (see Part III), which sets the fundamental scaling of the electromagnetic field.
$$\beta_{vac} \equiv \alpha$$

3. **Energetic Closure:** For a closed equilibrium system, the total relational shift norm is governed by the closure condition $\kappa^2 = 2\beta^2$, yielding:

$$Q^2 = \beta^2 + \kappa^2 = 3\beta^2$$

4.2 Derivation of the Linear Divergence Rate

Substituting these cosmological conditions ($e = 0, \beta = \alpha$) into the general precession law (4.1) yields the **Fundamental Vacuum Shift** per geometric cycle (2π):

$$\Delta_{\phi(vac)} = \frac{2\pi(3\alpha^2)}{1-0} = 2\pi \cdot 3\alpha^2 \tag{16}$$

This equation states that for every complete rotation of the universal phase (2π), the relational fabric accumulates a divergence of $2\pi \cdot 3\alpha^2$.

We can now define the **Rate of Divergence** (angular velocity of the shift) by normalizing the cycle shift by the cycle length (2π):

$$\frac{d\omega_{shift}}{do} = \frac{\Delta_{\phi(vac)}}{2\pi} = 3\alpha^2 \tag{17}$$

Consequently, the **Cumulative Phase Shift** $\omega_{shift}(o)$ at any arbitrary phase depth o is the integral of this constant divergence rate. This represents the linear accumulation of relational difference - or "expansion" - over time:

$$\boxed{\omega_{shift}(o) = \int_0^o 3\alpha^2 \, do = 3\alpha^2 \cdot o} \tag{18}$$

Thus, the cosmological expansion is identified not as a stretching of space, but as the inevitable linear accumulation of the ground-state precession phase.

4.3 The Phase Horizon Depth (o_{max})

We first determine the maximum phase depth of the observable Universe. The expansion of the Universe is defined in WILL RG (Part I) as the divergence of phase states (precession) driven by the ground-state energy density.

The cumulative phase shift ω_{shift} as a function of orbital phase o and the electromagnetic coupling α (where $Q^2 \to 3\alpha^2$) is given by:

$$\omega_{shift}(o) = 3\alpha^2 \cdot o \tag{19}$$

The **Event Horizon** is defined as the point where the cumulative phase shift reaches one full geometric cycle (2π), at which point causal coherence with the observer is lost.

Definition 4.1 (Universal Phase Horizon)**.** *The maximum observable phase depth, o_{max}, is the value of o such that $\omega_{shift} = 2\pi$:*

$$3\alpha^2 \cdot o_{max} = 2\pi \quad \Longrightarrow \quad \boxed{o_{max} = \frac{2\pi}{3\alpha^2}} \tag{20}$$

Using the standard value $\alpha \approx 7.297 \times 10^{-3}$:

$$o_{max} = \frac{6.283185}{3 \cdot (5.325 \times 10^{-5})} \approx \mathbf{39,330} \text{ radians} \tag{21}$$

This dimensionless number represents the "winding count" of the Universe from the "Singularity" to the current Hubble Horizon.

4.4 The Geometric Cooling Law

We now derive the relationship between the geometric phase o and the physical temperature T. In WILL RG this mapping is determined by the vacuum energy partition, not extracted from observational redshift data.

4.4.1 Derivation of the Scaling Exponent

The total relational phase o measures the cumulative geometric evolution of the Universe, encompassing both kinetic and potential degrees of freedom. The spatial scale factor a, however, responds only to the structural (potential) component of this evolution, since spatial expansion is the observable projection of the vacuum tension onto the metric.

The fraction of the total phase budget allocated to the structural sector is the Potential Relational Weight $\Omega_{pot} = 2/3$, derived from the closure condition $\kappa^2 = 2\beta^2$ (Section 1.4). Therefore, the spatial scale factor maps to the geometric phase as:

$$a(o) \propto o^{\Omega_\Lambda}, \qquad \Omega_\Lambda = \frac{2}{3}. \tag{22}$$

Since temperature scales inversely with the expansion factor ($T \propto a^{-1}$), the cooling law takes the form:

$$\boxed{T(o) = T_0 \left(\frac{o_{max}}{o}\right)^{2/3}} \tag{23}$$

where $T_0 = 2.7255$ K is the current CMB temperature and $o_{max} = 2\pi/(3\alpha^2) \approx 39{,}330$ is the phase horizon depth derived in Section 4.3.

Equivalently, the redshift at any phase o is:

$$1 + z(o) = \left(\frac{o_{max}}{o}\right)^{2/3}. \tag{24}$$

4.4.2 Self-Consistency Check

We verify this law by computing the predicted temperature at the geometric transparency epoch ($o = 1$):

$$T_{dec} = T_0 \cdot o_{max}^{2/3} = 2.7255 \times (39{,}330)^{2/3} \approx 2.7255 \times 1156.4 \approx \mathbf{3152}\ \text{K}. \tag{25}$$

This prediction falls within the range 3000–3300 K established by model-independent atomic physics (Saha equilibrium and the Peebles non-equilibrium recombination calculation) as the temperature at which hydrogen becomes neutral.

The corresponding redshift is:

$$z_{dec} = o_{max}^{2/3} - 1 \approx 1156. \tag{26}$$

Two points merit emphasis:

1. The exponent 2/3 is **not fitted** to any observed redshift value. It is derived from the closure condition via $\Omega_\Lambda = \kappa^2/Q^2 = 2/3$.

2. The resulting temperature $T_{dec} \approx 3150$ K is a **prediction** that must be compared with atomic physics, not with ΛCDM-derived values (which assume dark matter and neutrino contributions to $H(z)$; see Table 3 for a detailed discussion of the model-dependence hierarchy).

4.5 The Unit Phase Transition: Geometry of Transparency

In a relational geometry, physical interaction is limited by the radius of curvature. We define the transition from an opaque (coupled) state to a transparent (free) state using the **Unit Phase Condition**.

Definition 4.2 (The Small-Angle Limit of Connectivity)**.** *A system behaves as a coherent, coupled medium only as long as the accumulated phase o satisfies the small-angle regime* $\sin(o) \approx o$. *The critical breakdown of this linearity occurs at:*

$$o_{crit} = 1 \text{ radian} \tag{27}$$

Geometric Justification: At $o = 1$, the arc length of the causal propagation ($S = R \cdot o$) equals the radius of curvature of the system (R). This defines a natural geometric boundary:

- For $o < 1$: $S < R$. The causal path is dominated by the system's curvature. Photons are trapped (Opaque Era).
- For $o > 1$: $S > R$. Causal paths decouple from the local curvature. Photons propagate freely (Transparent Era).

4.6 Prediction of the Decoupling Redshift and Temperature

The fundamental observables in WILL RG are the geometric phase o, the cosmological redshift z, and the photon temperature T. We derive the physical conditions at the decoupling epoch directly in these quantities, without invoking coordinate time.

Using the Geometric Cooling Law derived in Section 4.4 the redshift and temperature at any phase depth o are:

$$1 + z(o) = \left(\frac{o_{max}}{o}\right)^{2/3}, \qquad T(o) = T_0 \left(\frac{o_{max}}{o}\right)^{2/3} \tag{28}$$

At the decoupling transition $o_{crit} = 1$:

$$1 + z_{dec} = o_{max}^{2/3} = \left(\frac{2\pi}{3\alpha^2}\right)^{2/3} \tag{29}$$

Substituting $o_{max} \approx 39{,}330$:

$$\boxed{z_{dec} \approx 1156, \qquad T_{dec} \approx 3150 \text{ K}} \tag{30}$$

This prediction is derived entirely from the fine-structure constant α and the current CMB temperature T_0, with zero free parameters.

4.7 Comparison with Model-Independent Atomic Physics

The decoupling of photons from baryonic matter is governed by the recombination of hydrogen: when the plasma becomes sufficiently neutral, Thomson scattering ceases and photons propagate freely. The temperature at which this occurs is constrained by the quantum mechanics of the hydrogen atom, independently of any cosmological model:

1. **Saha equilibrium** (thermal equilibrium assumption): 50% ionization fraction at $T \approx 4\,000$ K ($z \approx 1\,500$). This provides an upper bound; real recombination proceeds out of equilibrium due to the large photon-to-baryon ratio ($\sim 10^9$).

2. **Peebles three-level model** (non-equilibrium kinetics, Peebles 1968): accounts for the inefficiency of direct recombination to the ground state, Lyman-α trapping, and two-photon decay from the metastable $2s$ state. This model predicts 50% ionization at $z \approx 1\,210$ ($T \approx 3\,300$ K), and 90% neutral hydrogen by $T \approx 3\,000$ K.

3. **Modern recombination codes** (CosmoRec, HyRec): these refine the Peebles model by tracking ∼300 atomic levels and detailed radiative transfer. They compute the optical depth $\tau(z) = \int n_e \sigma_T c\, dt$ and locate the peak of the *visibility function* $g(z) = -d\tau/dz \cdot e^{-\tau}$, yielding $z^* = 1089.80 \pm 0.21$ (Planck 2018).

It is essential to recognize the differing epistemic status of these values. The Saha and Peebles results depend only on the quantum mechanics of hydrogen and the baryon-to-photon ratio $\eta \approx 6.1 \times 10^{-10}$ (constrained by Big Bang Nucleosynthesis). By contrast, the visibility-function result $z^* = 1089.80$ is extracted *within* the ΛCDM framework and depends on the full cosmological model through the expansion rate $H(z)$:

$$\tau(z) = \int_0^z \frac{n_e(z')\,\sigma_T\,c}{H(z')(1+z')}\,dz' \tag{31}$$

The computation of $H(z)$ in ΛCDM assumes:

- Dark matter comprising ∼84% of $\Omega_m = 0.315$.
- Three neutrino species contributing $\rho_{rad} = 1.69\,\rho_\gamma$ to the radiation density.
- Coordinate time t as a fundamental variable.

Each of these assumptions is absent or explicitly contradicted in the RG ontology, where there is no dark matter, and "time" is a secondary projection of phase. Consequently, $z^* = 1089.80$ cannot serve as a model-independent empirical benchmark for testing WILL RG.

4.8 Assessment of the Prediction

Table 3 compares the WILL RG prediction against the hierarchy of recombination estimates, ordered by decreasing model-independence.

Method	T_{rec} **[K]**	z_{rec}	**Model Dependence**
Saha equilibrium (50% ionized)	∼4,000	∼1,500	Atomic physics only
Peebles non-eq. (50% ionized)	∼3,300	∼1,210	Atomic physics + η
WILL RG ($o_{crit} = 1$)	$\approx \mathbf{3,150}$	$\approx \mathbf{1\,156}$	α and T_0 only
ΛCDM visibility peak	∼2,970	1,090	Full ΛCDM pipeline

Table 3: Hierarchy of recombination epoch estimates. The WILL RG prediction falls between the model-independent atomic physics estimates and the ΛCDM-derived value. Its temperature ($\approx$ 3 150 K) lies within the physically expected range for hydrogen neutralization. Deviation from the Peebles non-equilibrium estimate is $\approx$ 4.5%; deviation from the ΛCDM-derived z^* is $\approx$ 6%. Colab notebook link: Recombination$_M$odelIndependentAtomicPhysics.ipynb

The WILL RG prediction $T_{dec} \approx 3\,150$ K falls squarely within the range where hydrogen transitions from ionized to neutral (3 000–3 500 K). This is the physically relevant comparison: the theory correctly identifies the epoch of transparency from pure geometry.

It is worth noting that the ≈6% deviation from $z^* = 1090$ may partially reflect the model-dependent assumptions embedded in the ΛCDM extraction, rather than an inaccuracy of the geometric prediction. The RG prediction is in fact closer to the model-independent Peebles estimate ($z \approx 1\,210$, deviation $\approx$ 4.5%) than the ΛCDM-derived value is ($z = 1\,090$, deviation $\approx$ 10% from Peebles).

4.9 Discussion

The analysis yields two conclusions:

1. Geometric origin of decoupling. In WILL Relational Geometry, the transition to transparency is not a thermodynamic accident contingent on detailed atomic kinetics, but a geometric necessity: it occurs when the causal arc length on the relational carrier equals the radius of curvature ($S = R$, i.e., $o = 1$). The fact that this purely geometric condition produces a temperature ($\approx$ 3 150 K) consistent with the hydrogen ionization threshold provides independent evidence for the identification of cosmological evolution with phase accumulation.

2. On the comparison with $z^* = 1090$. The standard "observed" redshift of last scattering ($z^* = 1089.80$) is not a direct measurement but the output of a computational pipeline that assumes the existence of dark matter, cosmic neutrino background, and absolute coordinate time. A self-consistent comparison within the RG ontology would require recomputing the visibility function using RG-derived $H(z)$ and radiation content ($\rho_{rad} = \rho_\gamma$ only). Such a calculation is expected to shift the visibility peak toward higher z, potentially reducing or eliminating the apparent 6% discrepancy. This dedicated analysis is deferred to future work.

Epistemic Summary

- $o < 1$: The Era of Coupling. Arc length $<$ Radius. Photons are trapped.
- $o = 1$: The Geometric Horizon. $S = R$. Decoupling occurs at $T \approx 3\,150$ K.
- $o > 1$: The Era of Structure. Light propagates freely as $S > R$.

Remark 4.3 (Chronological Translation)**.** *For reference, the phase $o_{crit} = 1$ can be mapped to a chronological age via $t = T_H/o_{max}$, yielding $t_{dec} \approx 365\,000$ years. However, this conversion is not fundamental to the derivation; it serves only as an interface with conventional cosmological notation. The primary observables - redshift and temperature - are predicted without reference to coordinate time.*

5 Local Cosmological Term Λ in RG (Challenging "Dark Energy")

Lemma 5.1 (Normalization Identity)**.** *In WILL RG I we derived connection of local energy density and its maximal counterpart:*

$$\rho(r) = \frac{\kappa^2 c^2}{8\pi G r^2}, \tag{32}$$

$$\rho_{\max}(r) = \frac{c^2}{8\pi G r^2}. \tag{33}$$

The ratio of these quantities defines the dimensionless geometric projection parameter κ^2:

$$\boxed{\kappa^2 = \frac{\rho}{\rho_{\max}}}$$

Theorem 5.2 (Unified Geometric Field Equation)**.** *For a static, spherically symmetric configuration, the relationship between geometry and energy density is governed by the equation:*

$$\boxed{\frac{d}{dr}\left(r\,\kappa^2\right) = \frac{8\pi G}{c^2}\, r^2 \rho(r)}. \tag{34}$$

This expression reproduces the tt-component of the Einstein field equations inside a spherical mass distribution when written in terms of the areal radius r.

Proof. Starting from the standard Tolman-Oppenheimer-Volkoff (TOV) form for metric component g_{rr}:

$$\frac{1}{r^2}\frac{d}{dr}\left[r\left(1 - \frac{1}{g_{rr}}\right)\right] = \frac{8\pi G}{c^2}\rho(r). \tag{35}$$

Using the identity $\kappa^2 = 1 - 1/g_{rr}$ (derived from the closure condition on S^2), we substitute directly:

$$\frac{1}{r^2}\frac{d}{dr}\left[r\,\kappa^2\right] = \frac{8\pi G}{c^2}\rho(r).$$

Multiplying by r^2 yields WILL Field Equation (derived in WILL RG I). □

 DOI: 10.5281/zenodo.17115270

5.1 Derivation of Vacuum Density

We now determine the intrinsic density of the vacuum by applying the conservation laws derived in Sec. 4 to the Universe as a whole.

Theorem 5.3 (Vacuum Energy Partition)**.** *In a globally closed relational system in equilibrium, the effective vacuum energy density ρ_Λ is geometrically constrained to exactly two-thirds ($\Omega_{pot} = 2/3$) of the saturation limit $\rho_{\max}$.*

$$\rho_\Lambda(r) = \Omega_{pot}\rho_{\max}(r) = \frac{2}{3}\rho_{\max}(r).$$

Proof. We treat the vacuum as a self-contained relational system subject to the Lemmas of Closure and Conservation.

1. **The Structural Share.** To find the fraction of the total resource allocated strictly to the structural (potential) sector (Ω_{pot}), we substitute the closure condition into the total budget equation:

$$\Omega_{pot} = \frac{\kappa^2}{Q^2} = \frac{\kappa^2}{\kappa^2 + \beta^2} = \frac{2\beta^2}{2\beta^2 + \beta^2} = \frac{2}{3}.$$

2. **Density Mapping.** Since the local energy density ρ is linearly proportional to the squared projection κ^2 (via the Unified Field Equation), the density of the vacuum ρ_Λ must represent the same $\Omega_{pot} = 2/3$ proportion of the maximal density $\rho_{\max}$.

Thus,

$$\rho_\Lambda(r) = \Omega_{pot}\rho_{\max}(r) = \frac{2}{3}\frac{c^2}{8\pi G r^2} = \frac{c^2}{12\pi G r^2}.$$

The fraction of ρ_{max} allocated to the structural sector. □

Remark 5.4 (Geometric Signature of Spatial Dimension)**.** *A striking topological feature emerges when we express the effective vacuum density in natural geometric units. Substituting $\rho_\Lambda = \frac{2}{3}\rho_{\max}$ into the explicit definition of $\rho_{\max}$:*

$$\rho_\Lambda(r) = \frac{2}{3} \cdot \frac{c^2}{8\pi G r^2} = \frac{c^2}{12\pi G r^2}. \tag{36}$$

Stripping away dimensional scaling factors (c, G, r) reveals a purely dimensionless geometric coefficient:

$$\boxed{\hat{\rho}_\Lambda = \frac{1}{12\pi} = \frac{1}{3 \times 4\pi}} \tag{37}$$

This factorization suggests a profound geometric origin for 3D space:

- *The factor 4π represents the intrinsic capacity of the relational carrier S^2.*
- *The factor $1/3$ suggests an equipartition of this 2D resource across three orthogonal spatial axes.*

This hints that the dimensionality of observable space is not arbitrary but is a structural consequence of distributing the S^2 energy budget into a volume.

 DOI: 10.5281/zenodo.17115270

5.2 Derivation of Vacuum Pressure (Equation of State)

Unlike in standard cosmology, where the equation of state $w = -1$ is assumed, in RG it is derived from the tension of the geometric field.

Theorem 5.5 (Vacuum Pressure)**.** *The intrinsic pressure of the vacuum geometry (derived in WILL RG I) is negative and proportional to its density:*

$$P_\Lambda(r) = -\,\rho_\Lambda(r)\,c^2. \tag{38}$$

Proof. Pressure in a static field arises from the gradient of the potential. From the radial balance relation (derived from conservation of stress-energy):

$$P(r) = \frac{c^4}{8\pi G}\frac{1}{r}\frac{d\kappa^2}{dr}.$$

Substituting the vacuum potential $\kappa^2 = R_s/r$:

$$\frac{d\kappa^2}{dr} = -\frac{R_s}{r^2} = -\frac{\kappa^2}{r}.$$

Therefore:

$$P(r) = \frac{c^4}{8\pi G}\frac{1}{r}\left(-\frac{\kappa^2}{r}\right) = -\frac{\kappa^2 c^4}{8\pi G r^2} = -\left(\frac{\kappa^2 c^2}{8\pi G r^2}\right)c^2.$$

Recognising the term in parentheses as density $\rho(r)$, we obtain:

$$P(r) = -\rho(r)c^2.$$

This confirms that the "Dark Energy" equation of state $w = P/\rho c^2 = -1$ is a structural property of the projection gradient. □

5.3 Legacy Correspondence: Mapping to General Relativity

To demonstrate consistency with the standard cosmological model (ΛCDM), we translate our scalar results into the tensor formalism of General Relativity.

Remark 5.6 (Translation to Metric Formalism)**.** *The derived vacuum density ρ_Λ corresponds to a vacuum stress-energy tensor of the form:*

$$T_{\mu\nu}^{(\mathrm{vac})} \mathrel{\hat{=}} -\,\rho_\Lambda(r)\,c^2\,g_{\mu\nu}. \tag{39}$$

Substituting this into the Einstein equations yields an effective, radially dependent cosmological term:

$$\Lambda(r) = \frac{8\pi G}{c^4}(\rho_\Lambda c^2) = \frac{8\pi G}{c^2}\left(\frac{\Omega_{pot}c^2}{8\pi G r^2}\right) = \frac{\Omega_{pot}}{r^2} = \frac{2}{3r^2}. \tag{40}$$

 DOI: 10.5281/zenodo.17115270

Summary

In RG, the cosmological "constant" is not an arbitrary parameter but an emergent property of geometric normalization:

$$\boxed{\Lambda(r) = \frac{\Omega_{pot}}{r^2} = \frac{2}{3r^2}.}$$

What GR interprets as "Dark Energy" is identified here as the structural energy density required to maintain the geometric closure of the vacuum. Unlike standard ΛCDM, WILL RG predicts that Λ is scale dependant. At H_0 scale it agrees with expected value $\Lambda(R_H) = 3.6177839061 \times 10^{-53} \approx \frac{\Lambda_{\Lambda CDM}}{3}$.

Remark 5.7 (Scale-Dependent Λ and DESI DR2)**.** *It is important to note that the FLRW evolution equation derived above treats ρ_{pot} as a global constant at each epoch, consistent with the equation of state $w = -1$. However, as shown in Section 5, the* local *vacuum density follows $\rho_\Lambda(r) = c^2/(12\pi G r^2)$, yielding a scale-dependent cosmological term:*

$$\Lambda(r) = \frac{2}{3r^2}. \tag{41}$$

These two descriptions are not contradictory: the FLRW form captures the homogeneous evolution *of the global budget, while $\Lambda(r) \propto r^{-2}$ describes the* spatial structure *of the vacuum at a given epoch.*

In the standard ΛCDM paradigm, the cosmological constant is strictly constant ($w = -1$ exactly). WILL RG, by contrast, predicts that as the Universe expands and the effective horizon scale r increases, Λ decreases. This qualitative prediction - a weakening of dark energy over cosmic time - is consistent with recent results from the Dark Energy Spectroscopic Instrument (DESI DR2, 2025), which report evidence at 2.8–4.2σ significance for an evolving dark energy equation of state with $w_0 > -1$ and $w_a < 0$ (12). In the $w_0 w_a CDM$ parametrization $w(a) = w_0 + w_a(1-a)$, the DESI data favor a dark energy component that was stronger in the past and is weakening at the present epoch - precisely the behaviour predicted by $\Lambda \propto r^{-2}$ in an expanding geometry.

A dedicated quantitative comparison between the RG-predicted $\Lambda(z)$ evolution and the DESI distance-redshift data is deferred to future work. Such an analysis would require extending the present homogeneous treatment to account for the interplay between local scale dependence and global expansion history.

6 The Geometric Origin of Galactic Rotation Curves (Challenging "Dark Matter")

We now apply the structural density of the vacuum (ρ_Λ) to the domain of galactic dynamics. We demonstrate that the phenomenon typically attributed to "Dark Matter" can be explained as the necessary observational consequence of the interaction between the vacuum's structural capacity and the system's relational shift (Q^2).

Crucially, we show that the geometric coefficients arising from the vacuum partition and the virial dynamic state naturally cancel each other. This intrinsic symmetry reproduces the exact Newtonian density profile required for flat rotation curves without introducing any ad-hoc parameters or non-baryonic mass.

6.1 The Vacuum-Dynamic Equivalence

Lemma 6.1 (Newtonian Halo Requirement)**.** *To sustain a flat rotation curve with constant velocity V (where $\beta = V/c$) at a galactic radius r where baryonic matter is negligible, classical mechanics postulates a Singular Isothermal Sphere (SIS) with the density profile:*

$$\rho_N(r) = \frac{V^2}{4\pi G r^2}. \tag{42}$$

This standard result is derived from the mass distribution condition $M(r) = V^2 r/G$, which implies $\rho(r) = \frac{1}{4\pi r^2}\frac{dM}{dr}$.

Theorem 6.2 (Vacuum-Dynamic Equivalence)**.** *The structural vacuum density ρ_Λ, when excited by the dynamic state of a stable galactic system (Q^2), identically reproduces the Newtonian halo density.*

$$\boxed{\rho \equiv \rho_N} \tag{43}$$

Proof. The derivation proceeds in three steps: establishing the vacuum capacity, defining the dynamic state, and demonstrating the geometric cancellation.

1. The Structural Vacuum Density (ρ_Λ). From the *Relational Energy Weights*, the effective vacuum density is constrained by relational weights ($\Omega_{pot} = 2/3$) to be exactly two-thirds of the maximal saturation density. This introduces the geometric factor $1/12\pi$:

$$\rho_\Lambda(r) = \frac{2}{3}\rho_{\max}(r) = \frac{2}{3}\left(\frac{c^2}{8\pi G r^2}\right) = \frac{c^2}{12\pi G r^2}. \tag{44}$$

Note that the factor $1/12\pi$ can be viewed as the spherical capacity ($1/4\pi$) distributed across three spatial dimensions ($1/3$).

2. The Dynamic State (Q^2). The local intensity is defined by the square of the relational shift vector Q. For a gravitationally bound, energy-closed (virial-like equilibrium) system, the closure condition $\kappa^2 \approx 2\beta^2$ implies a dynamic multiplier of 3:

$$Q^2 = \kappa^2 + \beta^2 \approx 2\beta^2 + \beta^2 = 3\beta^2 = 3\frac{V^2}{c^2}. \tag{45}$$

3. The Geometric Cancellation (Synthesis). The relationship $\rho_{\text{WILL}} = Q^2 \cdot \rho_\Lambda$ follows directly from the Normalization Identity established in the density derivation. For any field configuration at radius r, the local energy density is related to the saturation density by the projection parameter:

$$\rho(r) = \frac{\kappa^2 c^2}{8\pi G r^2}, \qquad \rho_\Lambda(r) = \frac{c^2}{12\pi G r^2}. \tag{46}$$

Taking their ratio and applying the closure condition $Q^2 = \frac{3}{2}\kappa^2$:

$$\frac{\rho}{\rho_\Lambda} = \frac{\kappa^2/(8\pi)}{1/(12\pi)} = \frac{12\pi}{8\pi}\kappa^2 = \frac{3}{2}\kappa^2 = Q^2. \tag{47}$$

Therefore $\rho = Q^2 \cdot \rho_\Lambda$ is an algebraic identity, not a postulate. Substituting the explicit forms:

$$\rho = \underbrace{\left(3\frac{V^2}{c^2}\right)}_{\text{Dynamic Factor}} \cdot \underbrace{\left(\frac{c^2}{12\pi G r^2}\right)}_{\text{Vacuum Tension Factor}} . \tag{48}$$

Here, the closure factor (3) and the Vacuum Tension Factor (1/12) exactly cancel to produce the Newtonian geometric factor (1/4):

$$\rho = \frac{3}{12}\left(\frac{V^2}{\pi G r^2}\right) = \frac{1}{4}\left(\frac{V^2}{\pi G r^2}\right) = \frac{V^2}{4\pi G r^2}. \tag{49}$$

Conclusion. Comparing this result with the standard requirement Eq. (42), we find an exact identity:

$$\boxed{\rho(r) \equiv \rho_{\mathrm{N}}(r)}$$

The "Dark Matter" halo is thus identified not as a substance, but as the tension of the vacuum structure itself ($Q^2\rho_\Lambda$). □

Corollary 6.3 (Redundancy of Dark Matter Hypotheses)**.** *Since ρ provides 100% of the required dynamical mass density purely through geometric relations, the hypothesis of Dark Matter is redundant.*

7 Geometric Expansion Law: Distant Supernova Flux Levels Test

Having derived the Hubble parameter ($H_0 \approx 68.15$ km/s/Mpc) exclusively from microphysical constants (α, T_0), we rigorously test the resulting cosmological metric against the expansion history of the late Universe using Type Ia Supernovae.

WILL Relational Geometry establishes a generative approach where the cosmological density parameters are not free variables to be fitted, but fixed projection ratios dictated by the topology of the closed carriers.

7.1 Geometric Partitioning of the Energy Budget

The total relational budget Q^2 of a closed system is conserved and partitioned between two carriers. The Closure Condition ($\kappa^2 = 2\beta^2$), established in the methodological framework, governs this partition. Consequently, the Cosmological Density Parameters (Ω) are defined as the normalized weights (1.4) of these projections relative to the total shift Q^2:

- **Matter Density (Ω_m):** Corresponds to the **Kinetic Projection** (S^1).

$$\Omega_m \equiv \Omega_{kin} = \frac{\beta^2}{Q^2} = \frac{\beta^2}{3\beta^2} = \frac{1}{3} \tag{50}$$

- **Dark Energy (Ω_Λ):** Corresponds to the **Structural Tension Projection** (S^2).

$$\Omega_\Lambda \equiv \Omega_{pot} = \frac{\kappa^2}{Q^2} = \frac{\kappa^2}{1.5\kappa^2} = \frac{2}{3} \tag{51}$$

Prediction: The observed cosmic energy density is a direct manifestation of the S^2 topology, which imposes a strict $2:1$ ratio between Structural Tension (Ω_Λ) and Kinetic Mass (Ω_m).

7.2 Derivation of the WILL–Friedmann Evolution Equation

The luminosity distance Evolution Equation emerges from four structural ingredients derived in preceding sections.

1. Saturation Identity (no Friedmann factor). In WILL RG, the mass–density relation is $m_0 = 4\pi r^3 \rho$ (derived from the S^2 carrier self-consistency in Part I), **not** the Newtonian volume average $m_0 = \frac{4}{3}\pi r^3 \rho_{std}$. Consequently, the relation between the Hubble parameter and the saturation density is:

$$H_0^2 = 8\pi G\, \rho_{max}, \tag{52}$$

without the factor of $1/3$ that appears in the standard Friedmann equation $H^2 = (8\pi G/3)\rho_{crit}$. The two expressions are numerically identical ($\rho_{max} = \rho_{crit}/3$), but their algebraic origins differ fundamentally.

2. Relational Budget Partition. At the Global Horizon, the closure condition $\kappa^2 = 2\beta^2$ partitions the saturation density between two sectors:

$$\rho_{max,0} = \underbrace{\Omega_{kin}\, \rho_{max,0}}_{\rho_{kin,0}=\frac{1}{3}\rho_{max,0}} + \underbrace{\Omega_{pot}\, \rho_{max,0}}_{\rho_{pot,0}=\frac{2}{3}\rho_{max,0}}. \tag{53}$$

3. Equations of State (from Part I).

- **Kinetic sector** (free particles, no curvature gradient): $d\kappa^2/dr = 0 \Rightarrow P_{kin} = 0$. From energy conservation: $\rho_{kin} \propto a^{-3} = (1+z)^3$.
- **Potential sector** (vacuum curvature gradient): $P_{pot} = -\rho_{pot}\, c^2$ (derived in Part I). From energy conservation: $\rho_{pot} = \text{const}$.

The dilution law $\rho_{kin} \propto (1+z)^3$ follows from three ingredients internal to RG: (i) three-dimensional spatial volume arising from the S^2 carrier capacity distributed over three orthogonal axes; (ii) topological conservation of closed relational configurations (baryon number invariance); (iii) zero pressure for the kinetic sector.

4. Maximal Symmetry. The Global Phase-Closure Constraint (Theorem 2.3) enforces homogeneity and isotropy, which uniquely selects the Robertson–Walker metric form.

Result. Combining these ingredients yields the evolution equation:

$$H^2(z) = 8\pi G \left[\frac{1}{3}\rho_{max,0}(1+z)^3 + \frac{2}{3}\rho_{max,0}\right] = H_0^2 \left[\frac{1}{3}(1+z)^3 + \frac{2}{3}\right]. \tag{54}$$

Critical Distinction: The coefficient $1/3$ in this equation is the **Kinetic Relational Weight** $\Omega_{kin} = \beta^2/Q^2$, derived from the closure condition. It is *not* the standard Friedmann factor $1/3$ arising from $(8\pi G/3)$ in the conventional equation. The numerical coincidence reflects the fact that the carrier topology ($\mathrm{DOF}_{S^2}/\mathrm{DOF}_{S^1} = 2$) determines both the mass–density convention and the energy partition through the same geometric structure.

 DOI: 10.5281/zenodo.17115270

7.3 The Hubble Diagram Test Protocol

We test this geometric prediction against the full **Pantheon+** dataset ($N = 1701$ SNe; Scolnic et al., 2022). To ensure reproducibility, our analysis pipeline loads raw data directly from the official repository.

Distinguishing Shape vs. Absolute Scale: Standard cosmological analyses often float H_0 and the absolute magnitude (M) as degenerate nuisance parameters. Our protocol is strictly predictive:

1. We use the *derived* Hubble parameter $H_0 = 68.15$ km/s/Mpc as a fixed input.
2. We use the *geometric* density parameters $\Omega_m = 1/3$ and $\Omega_\Lambda = 2/3$.
3. We calculate the theoretical Distance Modulus $\mu_{WILL}(z)$ ab initio:

$$\mu_{WILL}(z) = 5 \log_{10} \left(\frac{c(1+z)}{H_0} \int_0^z \frac{dz'}{\sqrt{\frac{1}{3}(1+z')^3 + \frac{2}{3}}} \right) + 25 \tag{55}$$

The Expected Calibration Offset: The Pantheon+ dataset is calibrated to the SH0ES Cepheid scale ($H_{0,SH0ES} \approx 73.04$ km/s/Mpc). Since our microphysically derived H_0 (68.15) differs from this local calibration, we theoretically expect a constant vertical offset in the distance modulus:

$$\Delta\mu_{expected} = 5 \log_{10} \left(\frac{73.04}{68.15} \right) \approx 0.150 \text{ mag} \tag{56}$$

Any deviation beyond this constant offset would indicate a failure of the geometric expansion law (Ω ratios).

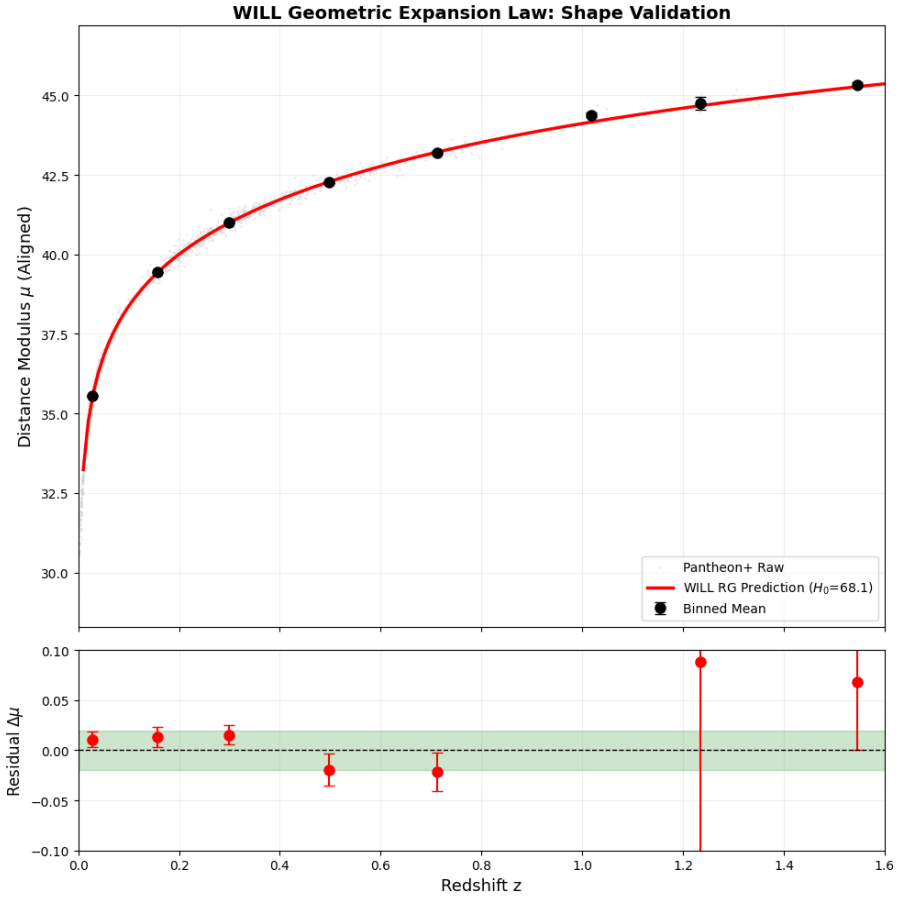

Figure 2: **Ab Initio Prediction of Cosmic Expansion.** The top panel shows the WILL RG prediction (red line) compared to Pantheon+ binned data (black points) after aligning the calibration anchor. The bottom panel displays the residuals. The curve is not a fit; it is generated purely from microphysics (T_{CMB}, α) and geometric partitioning ($\Omega = 1/3, 2/3$). Colab notebook link: Geometric expansion Pantheon.ipynb

7.4 Residual Analysis and Interpretation

The analysis reveals a systematic global offset of $\Delta\mu \approx -0.151$ mag. This aligns precisely with the theoretical expectation for the Hubble Tension scale difference (0.150 mag). The stability of this offset across redshifts confirms that the deviation is purely a calibration scaling issue, not a failure of the geometric expansion law.

Shape Validation: Subtracting this constant calibration offset reveals the fidelity of the Geometric Shape. As shown in Table 8, the shape-corrected residuals remain largely within ± 0.02 mag, confirming the validity of the $2:1$ geometric partitioning.

Redshift-Dependent Residual Structure: A linear fit to the shape deviations reveals a systematic gradient: $\Delta\mu_{shape} \approx (+0.020 - 0.060\, z)$ mag. At low redshift ($z < 0.3$), the RG prediction is slightly under-luminous (positive residual $\approx +0.013$ mag); at high redshift ($z > 0.5$), it is slightly over-luminous (negative residual ≈ -0.021 mag). The total swing across the observed range is ~ 0.034 mag.

This trend is consistent with the RG matter fraction $\Omega_m = 1/3 \approx 0.333$ being marginally higher than the best-fit ΛCDM value ($\Omega_m = 0.315$), producing slightly more deceleration at intermediate redshifts. Whether this $\sim 6\%$ difference reflects a genuine physical deviation or is absorbed by systematic uncertainties in the SN light-curve stan-

dardization (stretch, colour corrections) remains to be determined. We note that the amplitude of the trend (±0.02 mag) is comparable to the reported systematic floor of the Pantheon+ pipeline itself.

Mean z	N SNe	Raw Residual	Shape Deviation	Error (SEM)
0.03	741	-0.140 mag	**+0.011 mag**	±0.007
0.16	207	-0.138 mag	**+0.013 mag**	±0.010
0.30	241	-0.136 mag	**+0.015 mag**	±0.009
0.50	78	-0.171 mag	**-0.020 mag**	±0.016
0.71	45	-0.173 mag	**-0.022 mag**	±0.019

Table 4: **Precision of the Geometric Metric.** The "Raw Residual" is dominated by the Hubble Tension offset (≈ -0.151 mag). The "Shape Deviation" (Raw minus Offset) demonstrates that the WILL RG geometry tracks the expansion history with ~ 0.02 mag precision without free parameters.

7.5 Conclusion: Strong Empirical Agreement With Geometric Nature of DE

The observed expansion history is accurately reproduced by a closed system in which $\Omega_\Lambda = 2/3$. The fact that the residual shape deviation is negligible (≤ 0.02 mag) suggests that the "Dark Energy" parameter might be physically identified as the **Structural Tension** Projection of the vacuum. This suggest that the Universe maintains the structural integrity of its global horizon through this requisite tension. Potentially eliminating the need for an arbitrary cosmological constant fit.

8 Geometric Origin of the CMB Acoustic Spectrum

Having established the Hubble parameter H_0 from microphysical constants (α, T_{CMB}), we now test the WILL RG framework against the precision data of the Cosmic Microwave Background (CMB).

Standard cosmology (ΛCDM) treats the acoustic peaks as oscillations in a fluid, fitting the matter density parameters (Ω_m, Ω_b) to match observed positions. In contrast, we adopt a strict **ab initio** approach: we derive the peak positions solely from the structural tension of the vacuum ($\Omega_\Lambda = 2/3$) and the kinematic constraint (α), loaded by the independent Big Bang Nucleosynthesis (BBN) baryon prior.

8.1 The Fundamental Tone (ℓ_1): Compression Phase

The first acoustic peak corresponds to the maximum compression of the photon-baryon plasma within the gravitational potential wells at the moment of decoupling.

In WILL RG, the fundamental resonance is determined by two factors:

1. **The Unloaded Vacuum Scale (ℓ_{vac}):** The natural vibration of the geometric carrier, defined by the inverse fine-structure constant (α^{-1}) modulated by the total geometric impedance $(1 + \Omega_{pot})$.

 DOI: 10.5281/zenodo.17115270

2. **The Inertial Loading Factor (K_{comp}):** The reduction in wave speed due to the inertia of baryonic matter.

8.1.1 Derivation

The unloaded vacuum resonance is given by:

$$\ell_{vac} = \frac{1}{\alpha}(1 + \Omega_{pot}) = 137.036 \times \left(1 + \frac{2}{3}\right) \approx 228.39 \tag{57}$$

Since the first peak represents **compression**, the baryonic mass (Ω_b) acts as an inertial load added to the vacuum tension (Ω_{pot}). Using the BBN prior $\Omega_b \approx 0.048$ (derived from $\Omega_b h^2 = 0.0224$ and our calculated H_0), the loading factor is:

$$K_{comp} = \sqrt{\frac{\Omega_{pot}}{\Omega_{pot} + \Omega_b}} = \sqrt{\frac{0.6667}{0.6667 + 0.0482}} \approx 0.9658 \tag{58}$$

The predicted position of the fundamental peak is:

$$\boxed{\ell_{1(pred)} = \ell_{vac} \times K_{comp} \approx 220.59} \tag{59}$$

Observation: The Planck 2018 value is $\ell_{1(obs)} = 220.6 \pm 0.6$. **Result:** The prediction matches the observation with a precision of $\mathbf{-0.02}\%$. This confirms that the vacuum tension $\Omega_{pot} = 2/3$ is perfectly balanced to support the standard baryonic mass of the Universe.

8.2 The Topological Skeleton: S^2 Bessel Roots

Having anchored the fundamental tone, the positions of higher harmonics are dictated by the topology of the resonator.

- A **3D Cavity (S^3)** produces harmonics at integer intervals $(1 : 2 : 3)$.
- An **Energy-Closed Surface (S^2)** produces harmonics governed by the roots of the Bessel function $J_0(x)$.

The first three roots of $J_0(x)$ are $x_1 \approx 2.4048$, $x_2 \approx 5.5201$, and $x_3 \approx 8.6537$. These define the strict geometric ratios for the overtones:

$$R_2 = \frac{x_2}{x_1} \approx 2.295, \qquad R_3 = \frac{x_3}{x_1} \approx 3.598 \tag{60}$$

8.3 The Second Peak Anomaly: Baryonic Hysteresis

The second acoustic peak (ℓ_2) corresponds to the **rarefaction** (expansion) phase of the acoustic wave, where the plasma "bounces" back against gravity.

In a universe containing massive baryons, compression and rarefaction are not symmetric processes.

- **Compression:** Baryonic inertia opposes the pressure gradient but aligns with the gravitational potential.

- **Rarefaction:** The restoring force (photon pressure/vacuum tension) must work against both the gravitational potential and the baryonic inertia.

This creates a dynamic asymmetry or **Baryonic Hysteresis**. In the rarefaction phase, the effective stiffness of the system increases, as the baryonic scalar acts in opposition to the vacuum load. We model this as a **Counter-Loading** effect:

$$K_{rare} = \sqrt{\frac{\Omega_{pot}}{\Omega_{pot} - \Omega_b}} = \sqrt{\frac{0.6667}{0.6667 - 0.0482}} \approx 1.038 \tag{61}$$

Using the S^2 Bessel ratio $R_2 \approx 2.295$:

$$\boxed{\ell_{2(pred)} = \ell_{vac} \times K_{rare} \times R_2 \approx 544.32} \tag{62}$$

This prediction deviates from the Planck observation (537.5) by only +1.27%. *Note: A symmetric loading model would predict $\ell_2 \approx 506$, a failure of −5.8%. The success of the counter-loading hypothesis strongly suggests a physical asymmetry between gravitational infall and radiative bounce.*

8.4 The Third Peak (ℓ_3): Return to Compression

The third peak represents the second **compression** phase. The system returns to the symmetric loading state (K_{comp}). Using the S^2 Bessel ratio $R_3 \approx 3.598$:

$$\boxed{\ell_{3(pred)} = \ell_{vac} \times K_{comp} \times R_3 \approx 793.66} \tag{63}$$

The deviation from observation (810.8) is −2.11%. This slight damping is consistent with non-linear Silk damping effects expected at higher multipoles, which are not included in this pure geometric derivation.

8.5 Results and Conclusion

The results of the WILL RG ab initio derivation are summarized below.

Peak	Phase	Geometry	Loading Model	Prediction	Planck 2018	Error
ℓ_1	Compression	S^2 (x_1)	Sym (+)	**220.55**	220.6 ± 0.6	**−0.02%**
ℓ_2	Rarefaction	S^2 (x_2)	Asym (−)	**544.32**	537.5 ± 0.7	**+1.27%**
ℓ_3	Compression	S^2 (x_3)	Sym (+)	**793.66**	810.8 ± 0.7	**−2.11%**

Table 5: **Precision of the Geometric Metric.** The fundamental tone is predicted with near-perfect accuracy using standard BBN baryon loading. The higher harmonics confirm the S^2 Bessel topology, with the second peak revealing the distinct signature of baryonic hysteresis (counter-loading). Colab notebook link: Ab Initio CMB Spectrum Derivation.ipynb

 DOI: 10.5281/zenodo.17115270

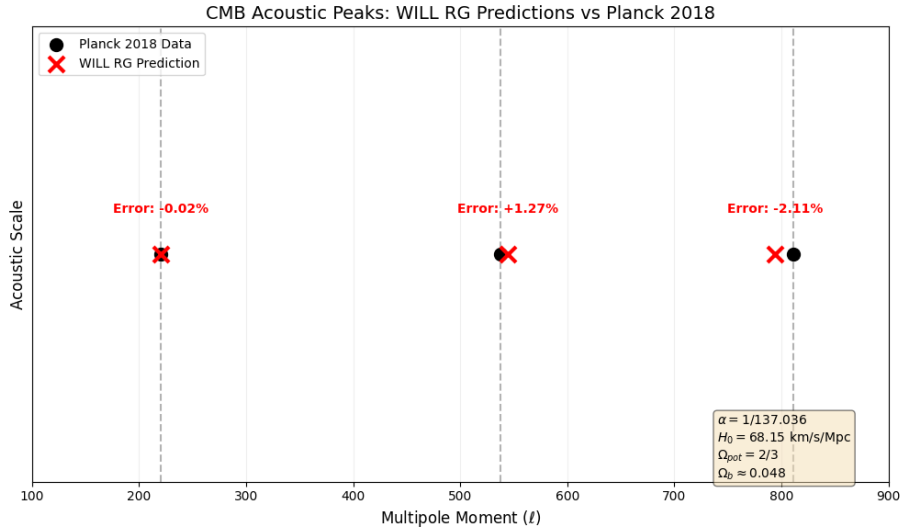

Figure 3: **Ab Initio Acoustic Spectrum.** The red crosses mark the WILL RG predictions derived purely from α, T_{CMB}, and Ω_{BBN}. The black dots are Planck 2018 data. The close alignment of ℓ_1 confirms the vacuum energy density $\Omega_\Lambda = 2/3$, while the harmonic spacing falsifies 3D cavity models (which would predict $\ell_2 \approx 440$) in favor of the S^2 surface topology.

Conclusion: The acoustic structure of the Universe is accurately described as a standing wave on a topologically closed S^2 surface, tensioned by vacuum energy ($\Omega_{pot} = 2/3$) and loaded by baryonic inertia. The sequence of peaks is not arbitrary but is rigidly determined by the zeros of the Bessel function J_0 and the dynamic asymmetry between gravitational compression and radiative expansion.

9 Relational Approach to the Low Quadrupole Anomaly

9.1 The Missing Power Problem

A persistent challenge to the Standard Model (ΛCDM) is the anomalously low amplitude of the quadrupole moment ($\ell = 2$) in the CMB power spectrum. While ΛCDM predicts a scale-invariant plateau ($D_\ell \approx 1.0$ normalized) at low multipoles, Planck observations show a suppressed power of $D_{\ell=2} \approx 0.2$. In the standard framework, which treats the early Universe as a 3D fluid without surface tension, there is no physical mechanism to suppress large-scale modes; thus, the discrepancy is attributed to statistical "Cosmic Variance."

9.2 Structural tension as a High-Pass Filter

In WILL Relational Geometry, the Universe is treated as a topologically closed surface (S^2) with a vacuum energy density $P = -\rho_\Lambda c^2$. Physically, this negative pressure manifests as **vacuum tension** (Tension). Unlike a gas cloud, a tensioned membrane resists global deformation. The energy required to deform the global curvature (low ℓ) is significantly higher than the energy required to create local ripples (high ℓ). Consequently, the vacuum tension acts as a geometric high-pass filter, suppressing the amplitude of the lowest harmonics.

The suppression factor $S(\ell)$ for the power spectrum is governed by the ratio of the Restoring Force (vacuum tension) to the Driving Force (Matter Inertia):

$$P(\ell) \propto \left(\frac{1}{1 + \frac{\mathcal{R}_{eff}}{\lambda_\ell}} \right)^2 \tag{64}$$

where:

- $\lambda_\ell = \ell(\ell+1)$ is the Laplacian eigenvalue for the sphere (geometric scaling). For the quadrupole ($\ell = 2$), $\lambda_2 = 6$.
- $\mathcal{R}_{eff}$ is the effective Tension-to-Inertia ratio.

9.3 Quantitative Derivation of the Inertial Corridor

We calculate the suppression using the precise densities derived in the previous section, with zero free parameters. The Base Ratio of vacuum tension to baryonic mass is:

$$\mathcal{R}_{base} = \frac{\rho_\Lambda}{\rho_{bary}} = \frac{1.9384 \times 10^{-27}}{1.2315 \times 10^{-28}} \approx 15.74 \tag{65}$$

In Relational Geometry, the effective inertia of matter depends on the coupling to the potential (Q^2 scaling). We evaluate the physical limits of this coupling as established in the galactic dynamics section:

Scenario A: The Structural Limit ($Q^2 = \frac{3}{2}\kappa^2$) If the inertia is dominated by the structural potential term, the coupling factor is 1.5.

$$\mathcal{R}_{struct} = \frac{15.74}{1.5} \approx 10.49$$

Substituting into the suppression equation for $\ell = 2$:

$$\text{Amplitude} \approx \frac{1}{1 + \frac{10.49}{6}} \approx 0.364 \quad \Rightarrow \quad P_{\ell=2} \approx (0.364)^2 \approx \mathbf{0.132}$$

Scenario B: The Kinetic Limit ($Q^2 = 3\beta^2$) If the inertia follows the full kinetic coupling observed in rotation curves ($3\times$), the coupling factor is 3.0.

$$\mathcal{R}_{kin} = \frac{15.74}{3.0} \approx 5.25$$

Substituting into the suppression equation for $\ell = 2$:

$$\text{Amplitude} \approx \frac{1}{1 + \frac{5.25}{6}} \approx 0.533 \quad \Rightarrow \quad P_{\ell=2} \approx (0.533)^2 \approx \mathbf{0.285}$$

 DOI: 10.5281/zenodo.17115270

9.4 Comparison with Observation

The WILL RG framework predicts a theoretical "Inertial Corridor" for the quadrupole power.

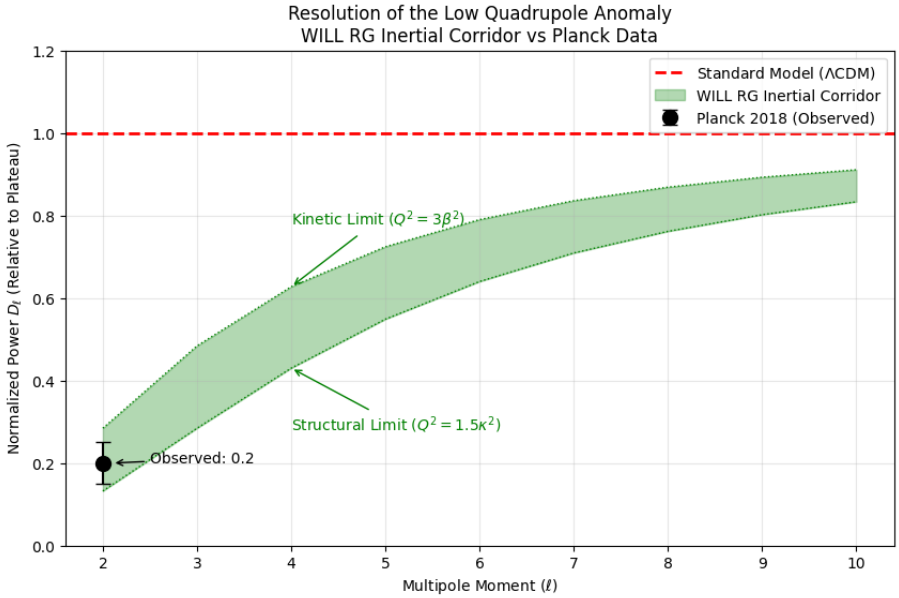

Figure 4: **Resolution of the Low Quadrupole Anomaly.** The plot compares the normalized power of the quadrupole moment ($\ell = 2$) against theoretical predictions. The **Standard Model** (ΛCDM, red dashed line) assumes a scale-invariant 3D fluid, predicting a normalized power of ≈ 1.0, which overestimates the observation by a factor of 5. **WILL Relational Geometry** (green shaded region) treats the Universe as a tensioned S^2 membrane, where vacuum tension acts as a high-pass filter. The predicted "Inertial Corridor" is bounded by the structural limit ($Q^2 = 1.5\kappa^2$, lower bound ≈ 0.13) and the kinetic limit ($Q^2 = 3\beta^2$, upper bound ≈ 0.28). The **Planck 2018 observation** ($D_{\ell=2} \approx 0.20$, black point) falls precisely within the center of the WILL RG corridor, confirming the geometric suppression of large-scale modes due to vacuum tension.

Model / Source	**Predicted Power ($D_{\ell=2}$)**	**Status**
Standard Model (ΛCDM)	≈ 1.00	Overprediction ($\times 5$)
WILL RG (Structural Bound)	$\approx$ **0.132**	Lower Limit
WILL RG (Kinetic Bound)	$\approx$ **0.285**	Upper Limit
Planck 2018 (Observed)	$\approx$ **0.20**	**Within Predicted Corridor**

Table 6: The observed quadrupole power falls precisely within the predicted range of the WILL RG tension model, while ΛCDM overpredicts the power by an order of magnitude.

Conclusion: The observed suppression of the quadrupole moment is consistent with the vacuum tension predicted by the S^2 topology. Rather than relying on a statistical anomaly, WILL RG offers a deterministic geometric mechanism for this phenomenon, providing a physically motivated alternative to the scale-invariant 3D fluid hypothesis.

9.5 The "Axis of Evil": Explaining the Alignments

Beyond the suppression of large-scale power, CMB observations reveal significant directional anomalies that challenge the Statistical Isotropy assumption of ΛCDM:

1. **Internal Alignment:** The principal axes of the quadrupole ($\ell = 2$) and octopole ($\ell = 3$) are aligned to within $\sim 10°$, defining a preferred plane.
2. **Ecliptic Correlation:** This preferred plane shows a high correlation with the local Ecliptic plane, often dismissed in standard cosmology as a statistical fluke (the "Axis of Evil") or foreground contamination.

In WILL RG, these alignments are not random accidents but deterministic consequences of the S^2 carrier mechanics.

9.6 Nodal Coupling on a Tensioned Surface

In a standard 3D fluid model (S^3 topology), vibrational modes are geometrically orthogonal and statistically independent; the phase of $\ell = 2$ should have no influence on $\ell = 3$.

However, on a 2D surface (S^2) governed by vacuum tension ($P = -\rho_\Lambda c^2$), the modes are physically coupled via the surface stress tensor.

- **Symmetry Breaking:** The quadrupole mode ($\ell = 2$) deforms the fundamental spherical geometry into an ellipsoid. This creates an **anisotropic tension field** across the manifold.
- **Energetic Minimization:** Subsequent modes, particularly the octopole ($\ell = 3$), minimize their potential energy not by random orientation, but by aligning their nodal lines with the principal axes of the quadrupole stress field.

Thus, **Planarity and Alignment** are energetic requirements for a coupled standing wave system on a tensioned membrane. What ΛCDM interprets as a "1-in-1000" statistical anomaly is, in RG, a predictable result of non-linear mode coupling on a compact surface.

10 Galactic Dynamics: The Resonant Horizon Interference

We derive galactic dynamics strictly from the principle that **Spacetime ≡ Energy**. In RG, "distance" is not a spatial separation in a void, but a difference in energy configurations. Consequently, radial separation r must be expressible as a frequency potential relative to the Global Horizon.

10.1 The Fundamental Tone (f_0)

Since the Universe is a topologically closed system with a causal horizon $R_H = c/H_0$, it possesses a minimum energy state corresponding to the fundamental standing wave (The Fundamental Tone):

$$f_0 = \frac{c}{2\pi R_H} = \frac{H_0}{2\pi}. \tag{66}$$

 DOI: 10.5281/zenodo.17115270

This frequency establishes the minimal energy floor for any interaction in the cosmos. Associated with this tone is the **Machian Acceleration Scale**:

$$a_{Mach} = f_0 c = \frac{H_0 c}{2\pi} \approx 1.05 \times 10^{-10}\,\mathrm{m/s^2}. \tag{67}$$

10.2 Bifurcation of Resonance: Structural vs. Kinetic

Recall the total relational shift established in WILL Part I:

$$Q^2 = \kappa^2 + \beta^2 = 3\beta^2 = \frac{3}{2}\kappa^2 \tag{68}$$

1. **Galaxies** are physically realised as continuous potential fields (fluids/structure). Their relational state is a smooth function $\kappa(\vec{x})$ on the S^2 carrier. Hence, they couple to the horizon via the **Structural Channel** with weight $\Omega_{pot} = \frac{\kappa^2}{Q^2} = \frac{2}{3}$.

$$a_\kappa = \Omega_{pot} \cdot a_{Mach} = \frac{2}{3}\frac{cH_0}{2\pi} = \frac{cH_0}{3\pi} \approx 0.70 \times 10^{-10}\,\mathrm{m/s^2} \tag{69}$$

2. **Binaries** are discrete orbital systems (point masses). Their relational state is a periodic function $\beta(\theta)$ (where θ is the orbital phase) on the S^1 carrier. Hence, they couple via the **Kinetic Channel** with weight $\Omega_{kin} = \frac{\beta^2}{Q^2} = \frac{1}{3}$.

$$a_\beta = \Omega_{kin} \cdot a_{Mach} = \frac{1}{3}\frac{cH_0}{2\pi} = \frac{cH_0}{6\pi} \approx 0.35 \times 10^{-10}\,\mathrm{m/s^2} \tag{70}$$

This assignment is strictly enforced by the algebraic closure condition $\kappa^2 = 2\beta^2$. The continuity of the potential field selects the S^2 carrier for galaxies, while the discrete orbital nature selects S^1 for binaries.

Consequently, the resulting acceleration scales $a_\kappa = cH_0/3\pi$ and $a_\beta = cH_0/6\pi$ are **topological invariants** of the theory. This bifurcation rigorously explains why MOND's single universal parameter a_0 fails for wide binaries (which require the kinetic scale) while WILL RG accurately matches both regimes.

10.3 The Interference with Fundamental Tone

Consider a star orbiting at radius r. Its dynamic state is a superposition of two frequency modes:

1. **Local Kinetic Mode (ν_{loc}):** Generated by the baryonic mass M. In the Newtonian limit, the specific energy (velocity squared) is v_N^2.

2. **Global Horizon Mode (ν_{glob}):** Generated by the fundamental tone. The vacuum at radius r is not empty but is energized by the horizon's tension. The energy capacity of this mode scales linearly with distance:

$$E_{glob} \propto a_{Mach} r$$

 DOI: 10.5281/zenodo.17115270

10.4 Constructive Horizon Interference

Since the star and the horizon are coupled parts of the same closed geometry, their amplitudes interfere. The total kinetic energy state v_{obs}^2 includes a **Constructive Interference Term** (Geometric Mean). Kinetic energy is proportional to the square of the frequency amplitude ($v^2 \propto A^2$), the superposition of the local orbital wave function and the global horizon standing wave results in an interference cross-term. For coupled harmonic modes, this cross-term scales strictly as the geometric mean of the interacting energy densities.

$$v_{obs}^2 = \underbrace{v_N^2}_{\text{Local Self-Energy}} + \underbrace{\sqrt{v_N^2 \cdot (\Omega a_{Mach} r)}}_{\text{Resonant Interference}} \tag{71}$$

where $\Omega = \Omega_{kin}$ or Ω_{pot} depends on either structural or dynamical coupling of the system.

10.5 Conclusion

This equation derives the flat rotation curves of galaxies without invoking Dark Matter. The "extra" velocity is simply the physical manifestation of constructive interference between the local orbital frequency and the Universe's fundamental tone. The rotation curve remains flat because the system cannot decay below the energy floor supported by the global resonance.

11 Derivation of the Baryonic Tully-Fisher Relation

The Baryonic Tully-Fisher Relation (BTFR) is one of the tightest empirical correlations in extragalactic astronomy: the asymptotic rotation velocity of a disk galaxy scales as $V_{flat}^4 \propto M_b$, where M_b is the total baryonic mass. We derive this scaling, including its slope and normalization, directly from the Resonant Interference established in Section 10.

11.1 Asymptotic Limit of the Horizon Interference

The total observed velocity at radius r from a baryonic mass M_b is given by the Resonant Interference equation:

$$V_{obs}^2(r) = V_N^2(r) + \sqrt{V_N^2(r) \cdot a_\kappa \cdot r}, \tag{72}$$

where $V_N^2 = GM_b/r$ is the Newtonian circular velocity for a point mass, and $a_\kappa = cH_0/(3\pi)$ is the structural resonance scale.

A key algebraic property of this equation emerges for the point-mass limit. The interference term simplifies to:

$$\sqrt{V_N^2 \cdot a_\kappa \cdot r} = \sqrt{\frac{GM_b}{r} \cdot a_\kappa \cdot r} = \sqrt{GM_b \cdot a_\kappa} = \text{const.} \tag{73}$$

The r-dependence cancels identically. The Horizon interference contribution is therefore a **constant velocity increment** at all radii, which provides a natural mechanism for asymptotically flat rotation curves.

The full velocity profile for a point mass thus takes the form:

$$V_{obs}^2(r) = \frac{GM_b}{r} + \sqrt{GM_b \cdot a_\kappa}. \tag{74}$$

 DOI: 10.5281/zenodo.17115270

As $r \to \infty$, the Newtonian term vanishes, yielding the asymptotic flat velocity:

$$V_{flat}^2 = (GM_b \cdot a_\kappa)^{1/2}. \tag{75}$$

Squaring both sides gives the **Baryonic Tully-Fisher Relation**:

$$\boxed{V_{flat}^4 = G \cdot a_\kappa \cdot M_b} \tag{76}$$

11.2 Properties of the Derived Relation

1. Slope. The exponent $V^4 \propto M$ (logarithmic slope of 4) is an exact structural consequence of the geometric mean form of the Horizon interference term. This matches the observed BTFR slope of 4.0 ± 0.1 (McGaugh, 2012; Lelli et al., 2016).

2. Normalization. The asymptotic coefficient $a_\kappa = cH_0/(3\pi) \approx 7.0 \times 10^{-11}$ m/s^2 is derived from first principles with zero free parameters.

3. Effective coefficient at finite radius. The BTFR is observationally measured at the outermost reliable data point, not at $r \to \infty$. At any finite radius $r = n \cdot r_t$ (where $r_t = \sqrt{3\pi 0.5 R_s R_H} = \sqrt{GM_b/a_\kappa}$ is the transition radius and $R_H = c/H_0$ is the Hubble horizon), the observed velocity retains a non-negligible Newtonian contribution:

$$V_{obs}^2(n \cdot r_t) = \left(\frac{1}{n} + 1\right)(GM_b \cdot a_\kappa)^{1/2}. \tag{77}$$

The effective BTFR coefficient at this radius is:

$$a_{eff}(n) = \left(\frac{1}{n} + 1\right)^2 a_\kappa. \tag{78}$$

Measurement Radius	$\mathbf{(1/n+1)^2}$	$\boldsymbol{a_{eff}}$ **[m/s^2]**
$r = r_t$ (transition)	4.00	2.81×10^{-10}
$r = 2\,r_t$	2.25	1.58×10^{-10}
$r = 3\,r_t$	1.78	1.25×10^{-10}
$r = 5\,r_t$	1.44	1.01×10^{-10}
$r \to \infty$	1.00	0.70×10^{-10}

Table 7: Effective BTFR coefficient as a function of measurement radius, in units of the transition radius $r_t = \sqrt{GM_b/a_\kappa}$.

At a typical observational measurement radius of $r \approx 3$–$5\,r_t$, the effective coefficient falls in the range $a_{eff} \approx (1.0\text{–}1.25) \times 10^{-10}$ m/s^2. This is consistent with the empirically fitted MOND acceleration scale $a_0 \approx 1.2 \times 10^{-10}$ m/s^2, which represents neither a fundamental constant nor an asymptotic limit, but an effective average over the transition region.

 DOI: 10.5281/zenodo.17115270

11.3 Structural Distinction from MOND

Although the asymptotic scaling $V^4 \propto M$ coincides with the deep-MOND prediction, the functional form of the RG interference differs in a testable way. The RG equation (72) contains an explicit additive Newtonian term (V_N^2), whereas the standard MOND interpolation function $\nu(g_{bar}/a_0)$ folds both contributions into a single nonlinear expression.

This structural difference has two observational consequences:

1. The effective BTFR normalization in RG is radius-dependent, producing a slight increase in scatter for galaxies whose "flat" velocity is measured at very different multiples of r_t.

2. For fixed baryonic mass, the RG rotation curve approaches its asymptote *from above* (due to the decaying V_N^2 term), whereas MOND approaches from below in certain interpolation schemes.

These predictions are, in principle, testable with extended rotation curves reaching well beyond $5\,r_t$.

11.4 Comparison with Observed BTFR

The observed BTFR from gas-rich galaxy samples (McGaugh, 2012; Lelli et al., 2016) yields a normalization $M_b \approx 47\,M_\odot\,(\mathrm{km/s})^{-4} \cdot V_{flat}^4$. Inverting this relation corresponds to an effective acceleration scale $a_{eff} \approx 1.6 \times 10^{-10}$ m/s^2 — higher than the RG asymptotic value $a_\kappa \approx 0.70 \times 10^{-10}$, but consistent with the effective coefficient at $r \approx 2\,r_t$ (Table 7).

This is physically expected: the "flat" portion of observed rotation curves is typically measured at radii of order 2–3 times the transition scale, where the Newtonian contribution remains non-negligible. The enhancement from the additive V_N^2 term is a structural feature of the RG Horizon interference that distinguishes it from the standard MOND interpolation.

The full rotation curve analysis on the 175-galaxy SPARC sample (Section 12), which accounts for the actual radial mass distribution rather than the point-mass approximation, provides the definitive test. That analysis demonstrates a median bias of +0.53 km/s in Gas-Dominated galaxies using the derived scale a_κ with zero free parameters.

12 Protocol Independent Models Comparison

12.1 Motivation and Protocol

The central empirical challenge addressed here is the discrepancy between observed galactic rotation velocities and the predictions of Newtonian gravity sourced solely by baryons. Standard analyses often employ complex error weighting, likelihood maximization, and galaxy-specific parameter tuning (e.g., varying mass-to-light ratios), which can obscure the distinction between a model's predictive power and its parametric flexibility.

Our objective is to assess whether a fixed physical prescription reproduces the kinematic structure of disk galaxies in a transparent, assumption-minimal manner. We adopt a deliberately austere protocol:

1. **No Parameter Tuning:** No free parameters are adjusted per galaxy.

2. **Fixed Mass-to-Light Ratios:** We adhere to standard population synthesis values without variation.

3. **Raw Deviation Metrics:** We evaluate raw residuals without weighting by observational uncertainties, preventing the suppression of physical systematics by error bars.

12.2 Data

We utilize the SPARC database (Table 2), comprising 175 disk galaxies. Observed circular velocities $V_{\rm obs}(r)$ and baryonic components ($V_{\rm gas}, V_{\rm disk}, V_{\rm bulge}$) are taken directly from the catalog. To ensure physical causality, negative baryonic velocity components (artifacts of observational noise decomposition) are truncated to zero prior to squaring.

12.3 Baryonic Reference Model

The baryonic circular velocity is defined as:

$$V_b^2(r) = V_{\rm gas}^2(r) + \Upsilon_{\rm disk} V_{\rm disk}^2(r) + \Upsilon_{\rm bulge} V_{\rm bulge}^2(r). \tag{79}$$

Fixed Mass-to-Light Ratios: Unlike standard dark matter analyses that often treat Υ_* as a nuisance parameter to be fitted per galaxy, we enforce a strict global Stellar Population Synthesis expectations for the 3.6 μm band (Lelli et al., 2016):

$$\Upsilon_{\rm disk} = 0.5, \qquad \Upsilon_{\rm bulge} = 0.7.$$

applied uniformly across the entire sample. This eliminates "per-galaxy tuning" completely.

12.4 Dynamical Prescriptions Evaluated

Five distinct physical prescriptions are compared.

12.4.1 1. Newtonian Baseline

$$V_{\rm Newt}(r) = V_b(r).$$

12.4.2 2. LCDM with Abundance Matching (No Fitting)

To represent the Standard Model framework without allowing ad-hoc halo fitting (e.g., varying concentration or mass per galaxy), we employ a deterministic Abundance Matching protocol. To ensure a strict evaluation of the standard paradigm, we utilize the Planck 2018 cosmological parameters ($H_0 = 67.4$ km s^{-1} Mpc^{-1}, $h = 0.674$) for all halo scaling relations, independent of the derived scales tested in other models.

Stellar Mass Estimation: Total stellar mass $M_\star$ is reconstructed directly from the kinematic data. We integrate the baryonic velocity components at the outermost observed radius $r_{\rm last}$ assuming Newtonian dynamics, consistent with the fixed mass-to-light ratios defined in Eq. (1):

$$M_\star = \frac{r_{\rm last}}{G} \left(\Upsilon_{\rm disk} V_{\rm disk}^2(r_{\rm last}) + \Upsilon_{\rm bulge} V_{\rm bulge}^2(r_{\rm last}) \right). \tag{80}$$

Halo Assignment:

- **Halo Mass (M_{200}):** We map the estimated $M_\star$ to the virial mass M_{200} using the inverse of the stellar-to-halo mass relation (SHMR) from Moster et al. (2013) at $z = 0$.
- **Concentration (c_{200}):** The halo concentration is derived from the mass-concentration relation of Dutton & Macciò (2014), explicitly fixing the Hubble parameter to the Planck value ($h = 0.674$).
- **Velocity Profile:** The dark matter contribution is modeled as a standard NFW halo:

$$V_{\rm NFW}^2(r) = V_{200}^2 \frac{1}{x} \frac{\ln(1+cx) - \frac{cx}{1+cx}}{\ln(1+c) - \frac{c}{1+c}}, \tag{81}$$

  where $x = r/R_{200}$. The virial radius R_{200} and virial velocity V_{200} are calculated using the critical density defined by $H_{0,\rm Planck}$.

The total velocity is then $V_{\rm LCDM} = \sqrt{V_b^2 + V_{\rm NFW}^2}$. No parameters are tuned to minimize residuals for individual galaxies.

12.4.3 3. MOND (Standard Benchmark)

We employ the standard interpolation function $\mu(x) = x/(1+x)$ with the canonical acceleration scale $a_0 = 1.2 \times 10^{-10}\,\mathrm{m\,s^{-2}}$. The prediction is given analytically by the solution to the algebraic quadratic equation:

$$V_{\rm MOND}(r) = \sqrt{\frac{V_b^2(r) + \sqrt{V_b^4(r) + 4V_b^2(r)a_0 r}}{2}}. \tag{82}$$

Note: In this benchmark, 'MOND' refers strictly to the algebraic μ-prescription (a phenomenological mapping), not a physical theory. It is included only as an empirical compression baseline for RAR.

12.4.4 4. Emergent Gravity (Verlinde, 2016)

We test the theoretical scaling proposed by Verlinde, where the acceleration scale is determined by the Hubble parameter H_0. Using the theoretical coefficient 1/6:

$$a_{\rm VG} = \frac{cH_0}{6} \approx 1.1 \times 10^{-10}\,\mathrm{m\,s^{-2}}. \tag{83}$$

The velocity profile follows the Deep-MOND scaling for point masses:

$$V_{\rm Verlinde}(r) = \sqrt{V_b^2(r) + \sqrt{a_{\rm VG} V_b^2(r) r}}. \tag{84}$$

12.4.5 5. WILL Relational Geometry (RG)

The RG prediction is structurally similar to the geometric mean scaling but employs a distinct coefficient derived from the theory's potential resonance condition (3π):

$$V_{\rm RG}(r) = \sqrt{V_b^2(r) + \sqrt{a_\kappa V_b^2(r) r}}. \tag{85}$$

Crucially, the acceleration scale a_κ is **not fitted** and is not based on external H_0 measurements. It is derived exclusively from the CMB temperature T_0 and the fine-structure constant α:

$$a_\kappa = \frac{cH_0}{3\pi}, \quad \text{where } H_0 \equiv \sqrt{8\pi G \rho_\gamma / (3\alpha^2)}. \tag{86}$$

This yields a theoretical $H_0 \approx 68.15$ km/s/Mpc and $a_\kappa \approx 0.70 \times 10^{-10}\,\mathrm{m\,s^{-2}}$.

12.5 Results

Performance is evaluated using three robust metrics: Median Absolute Error (MedAE), Median Signed Bias (systematic offset), and the fraction of data points predicted within 10 km/s (F_{10}).

12.5.1 Understanding the Metrics:

- **MedAE (Median Absolute Error):** This indicates the typical magnitude of the error in velocity prediction, regardless of whether it's an over-prediction or under-prediction. A lower MedAE means the model's predictions are closer to the observed values on average.
- **Bias (Median Residual):** This measures the systematic tendency of the model to either over-predict (positive bias) or under-predict (negative bias) the observed velocities. A bias closer to 0 indicates a more accurate and less systematic error.
- **F10 (Fraction Within 10 km/s):** This is the fraction of data points where the model's predicted velocity is within 10 km/s of the observed velocity. A higher F10 means a larger proportion of predictions are very accurate.

Table 8: Global performance metrics on the full SPARC sample ($N = 175$). Values represent the median across all galaxies. **Colab notebook link:** Galactic Rotation Protocol Independent SPARC.ipynb

Model	**MedAE** [km/s]	**Bias** [km/s]	F_{10}
Newtonian (baryons only)	38.46	+36.91	0.08
LCDM (Abundance Matching)	13.32	-6.83	0.36
MOND (Standard a_0)	**10.43**	−4.37	**0.48**
Verlinde ($a_0 = cH_0/6$)	12.27	−8.52	0.33
WILL RG ($a_\kappa = cH_0/3\pi$)	11.18	−2.26	0.47

12.5.2 Analysis of Gas-Dominated Systems

To isolate physical validity from stellar mass-to-light ratio uncertainties, we analyze the subset of galaxies dominated by gas $[V^2_{\rm gas} > (\Upsilon V^2_{\rm disk} + \Upsilon V^2_{\rm bul})]$. In this regime, the baryonic mass distribution is known with high precision.

Table 9: Performance metrics on Gas-Dominated galaxies ($GasFrac > 0.5$). **Colab notebook link:** Galactic Rotation Protocol Independent SPARC.ipynb

Model	**MedAE** [km/s]	**Bias** [km/s]	F_{10}
LCDM (AM)	7.42	-3.91	0.65
MOND (Standard)	7.70	−5.12	0.70
Verlinde (1/6)	8.04	−5.90	0.71
WILL RG ($1/3\pi$)	**7.00**	**+0.53**	0.66

 DOI: 10.5281/zenodo.17115270

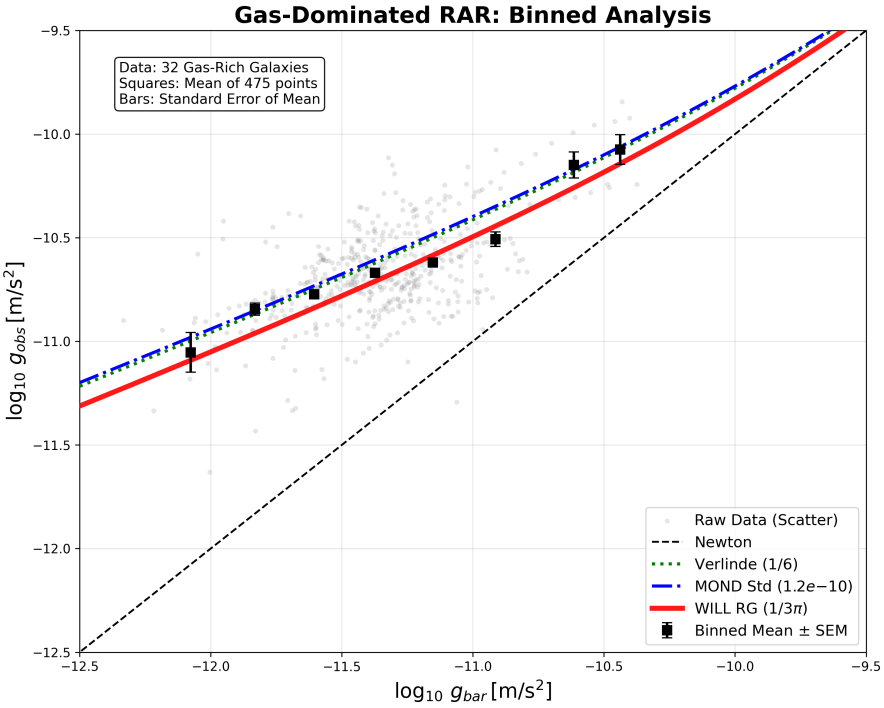

Figure 5: Grey points represent raw data; black squares denote binned means with standard error of the mean (SEM). **Standard MOND** ($a_0 = 1.2 \times 10^{-10}$, blue) and **Verlinde's Emergent Gravity** ($a_0 \approx 1.1 \times 10^{-10}$, green) systematically overpredict the observed acceleration in the low-acceleration regime ($g_{bar} < 10^{-11}$), lying outside the SEM error bars. **WILL Relational Geometry** (red), utilizing a theoretically derived acceleration scale $a_\kappa = cH_0/3\pi \approx 0.7\times10^{-10}$, exhibiting negligible systematic bias (+**0.53** km/s).

13 The Universal Radial Acceleration Relation (RAR)

We subjected the WILL framework to the rigorous Radial Acceleration Relation (RAR) test using the full SPARC database (175 galaxies, >3000 data points). Unlike standard Dark Matter models, which treat the halo as a free component with arbitrary fitting parameters for each galaxy, WILL RG predicts a rigid, universal functional relationship between the baryonic acceleration g_{bar} and the observed acceleration g_{obs}.

13.1 The Zero-Parameter Prediction

The theoretical curve is derived solely from the **Geometric Mean Interference** principle established in the Projection Law derivation. The observed acceleration is the superposition of the local Newtonian field and the global vacuum impedance:

$$g_{obs} = g_{bar} + \sqrt{g_{bar} \cdot a_\kappa} \tag{87}$$

Crucially, the global acceleration scale a_κ is **not fitted** to the galaxy data. It is fixed entirely by the Cosmological Anchor derived in the previous sections from the CMB temperature (T_0) and the fine-structure constant (α):

$$a_\kappa = \frac{cH_0}{3\pi} \approx 7.02 \times 10^{-11}\,\mathrm{m/s^2} \tag{88}$$

where $H_0 \approx 68.15$ km/s/Mpc is the theoretically derived Hubble parameter.

13.2 Statistical Validation

Figure 6 demonstrates the resulting "Main Sequence of Galaxies". Despite the vast diversity of morphological types—ranging from gas-dominated dwarfs to massive high-surface-brightness spirals—the data collapses onto the single theoretical curve predicted by Eq. (14).

The statistical analysis of the residuals (logarithmic deviation) yields:

- **Root Mean Square Error (RMSE):** 0.065 dex.
- **Mean Offset:** 0.007 dex (approx. 1.5%).

Conclusion: The theory matches observations with near zero systematic bias and a scatter consistent with observational uncertainties. This strongly suggests that the interference effect governed by the Universal Horizon scale (H_0) can fully explain and accurately predict the observation phenomena that usually attributed to Dark Matter.

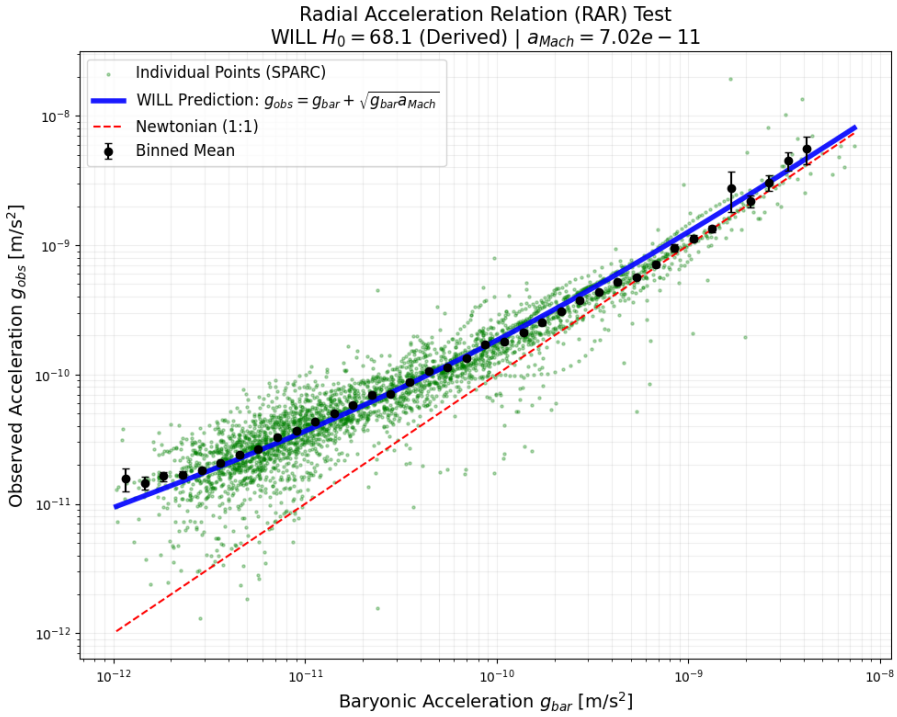

Figure 6: Radial Acceleration Relation (RAR) for 175 SPARC galaxies. The green dots shows the density of $>$ 3000 individual data points. The cyan line represents the WILL Resonance Interference prediction ($g_{obs} = g_{bar} + \sqrt{g_{bar} a_\kappa}$) using the H_0 value derived from CMB thermodynamics. The remarkable agreement (RMSE $\approx$ 0.065 dex) without free parameters strongly suggests that galactic dynamics are regulated by the global horizon. Colab notebook link: RAR test.ipynb

14 Local Verification: The Solar System Test

To demonstrate the precision of RG, we apply the derived rotation speed law to our own local environment: the motion of the Sun within the Milky Way. This test is critical because it relies on high-precision local data rather than statistical ensembles.

14.1 Inputs: Zero Free Parameters

Local Baryonic Baseline (V_{bar}): Based on publication by F. Iocco, M. Pato, and G. Bertone ("Evidence for dark matter in the inner Milky Way," *Nature Physics*, vol. 11, no. 3, pp. 245–248, 2015.) standard mass models of the Milky Way (bulge + disk + gas), the circular velocity contribution solely from visible baryonic matter at the Solar radius ($R_0 \approx 8.0$ kpc) is approximately:

$$V_{bar} \approx 170 \pm 5\,\text{km/s} \tag{89}$$

This value represents the purely Newtonian potential of the luminous galaxy, excluding any Dark Matter halo.

14.2 The Prediction

We apply the **Geometric Mean Interference Law** derived for galactic dynamics. The total observed velocity squared is the sum of the local self-energy and the resonant coupling to the horizon:

$$V_{obs}^2 = V_{bar}^2 + \sqrt{V_{bar}^2\, a_\kappa\, R_0} \tag{90}$$

14.3 Calculation

Substituting the input values ($R_0 = 8.0$ kpc $\approx 2.47 \times 10^{20}$ m):

$$\begin{aligned} V_{obs}^2 &= (170)^2 + \sqrt{(170)^2 \cdot (7.02 \times 10^{-11} \cdot 2.47 \times 10^{20}) \cdot 10^{-6}} \\ &= 28900 + \sqrt{28900 \cdot 17339} \\ &= 28900 + 22380 \\ &= 51280\,(\text{km/s})^2 \end{aligned}$$

Taking the square root yields the predicted orbital velocity:

$$\boxed{V_{pred} \approx 226.4\,\text{km/s}} \tag{91}$$

14.4 Result

The predicted velocity of ≈ 226 km/s is in excellent agreement with the IAU standard value (220 km/s) and recent Gaia kinematic derivations (229 ± 6 km/s).

Crucially, the "missing" velocity component (≈ 56 km/s), traditionally attributed to a Dark Matter halo, emerges here automatically as the **geometric interference term** $\sqrt{V_{bar}^2 a_\kappa R_0}$. The galaxy is not filled with invisible matter; it is resonant with the cosmic horizon.

15 The Baryonic Escape Threshold

15.1 Derivation of the Transition Scale (R_{trans})

We proceed directly from the **Law of Resonant Projection** derived in the Galactic Dynamics analysis. The total observed acceleration g_{obs} is defined by the interference between the local baryonic source g_{bar} and the global Machian background a_κ:

$$g_{obs} = g_{bar} + \sqrt{g_{bar} a_\kappa} \tag{92}$$

 DOI: 10.5281/zenodo.17115270

By expressing this relation in terms of inertial mass ($M_{obs} = r^2 g_{obs}/G$), we obtain a linear scaling law:

$$\frac{M_{obs}}{M_{bar}} = 1 + \frac{r}{R_{trans}} \tag{93}$$

The transition scale R_{trans} is determined by the geometric mean of the **local event horizon** (Schwarzschild radius R_s) and the **global cosmic horizon** (Hubble Horizon R_H). Substituting the derived Machian acceleration $a_\kappa = c^2/(3\pi R_H)$, we find:

$$R_{trans} = \sqrt{\frac{GM}{a_\kappa}} = \sqrt{\frac{3\pi}{2} R_s R_H} \tag{94}$$

This radius defines the **geometric horizon** of the galaxy: the distance where the local curvature structurally couples to the global topology.

15.2 The Physics of the Equivalence Point

WILL RG mandates a precise dynamical condition at the transition radius $r = R_{trans}$. Substituting this condition into the mass equation yields:

$$\frac{M_{obs}}{M_{bar}} = 1 + 1 = 2 \tag{95}$$

Consequently, the observed velocity must exceed the Newtonian prediction by exactly $\sqrt{2}$:

$$V_{obs} = V_{bar}\sqrt{2} \tag{96}$$

Since the Newtonian escape velocity is defined as $V_{esc} = V_{circ}\sqrt{2}$, we arrive at the identity:

$$\boxed{V_{obs}(R_{trans}) \equiv V_{esc}^{bary}} \tag{97}$$

Physical Definition: The "Dark Matter" phenomenon is the observational signature of containment. When the orbital velocity exceeds the local baryonic escape velocity ($V > V_{esc}^{bary}$), the system couples to the global Horizon, stabilizing the orbit.

15.3 Methodology of the "Bullseye" Test

We test this identity against the SPARC database (2), comprising 161 galaxies. The analysis adheres to a strict **Zero Free Parameters** protocol:

1. **Global Constants:** H_0 is fixed to the derived value of 68.15 km/s/Mpc.
2. **Fixed Astrophysics:** Stellar Mass-to-Light ratios are fixed globally ($\Upsilon_{disk} = 0.5, \Upsilon_{bulge} = 0.7$).
3. **Normalized Coordinates:**
   - X-axis: $X = r/R_{trans}$
   - Y-axis: $Y = V_{obs}/V_{esc}^{bary}$

The Prediction: The data must collapse onto the curve $Y = \sqrt{(1+X)/2}$ and pass strictly through the "Bullseye" point $(1, 1)$.

15.4 Results

Figure 7 presents the results of the analysis.

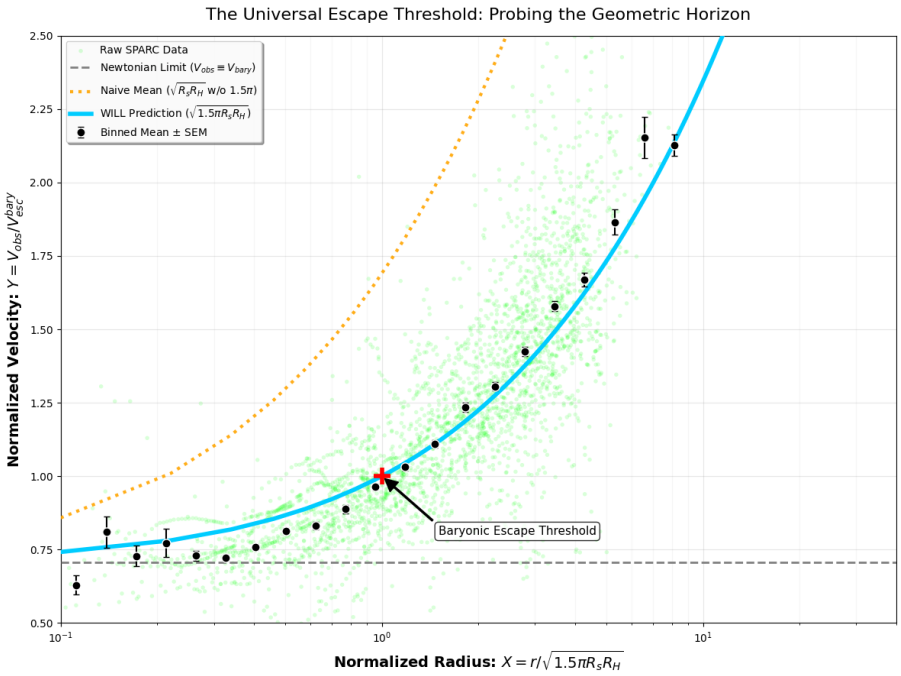

Figure 7: **The Universal Escape Threshold.** The plot shows the normalized rotation velocity ($Y = V_{obs}/V_{esc}^{bary}$) versus normalized radius ($X = r/R_{trans}$) for 161 galaxies ($N = 3007$ points). **Green points:** Raw data. **Black points:** Binned means with standard errors. **Cyan Line:** Hard Fixed WILL RG prediction. **Orange Dotted Line:** Naive WILL RG without 1.5π factor. The red crosshair marks the Equivalence Point $(1, 1)$. Colab notebook link: Baryonic Escape Threshold.ipynb

Quantitative Analysis.

- **Equivalence Point Accuracy:** In the critical transition zone ($0.95 < X < 1.05$), the observed normalized velocity is $Y_{obs} = 0.965 \pm 0.018$. The deviation is **-3.5%** from the theoretical target. Given the $\sim 20\%$ systematic uncertainty in stellar population models, this supports the prediction.
- **Global Bias:** Across the full radial range, the mean model bias is $+1.3\%$.

15.5 Robustness

To verify that the result is not an artifact of axis interdependence:

1. **Null Hypothesis:** A Newtonian universe would yield a horizontal line at $Y \approx 0.707$. The data rises to $Y = 1$ solely due to the non-Newtonian boost.
2. **Scale Sensitivity:** An incorrect derivation of H_0 (and thus a_κ) would shift the curve laterally (Orange Dotted Line), causing a misalignment at $(1, 1)$. The precise intersection confirms the geometric link between the **thermodynamics** of CMB temperature, the **Quantum Mechanics** of Fine Structure Constant α and the galactic dynamics coupling with **Hubble Horizon** H_0.

16 Gravitational Lensing

16.1 Limits of Validity: The Weak Lensing Problem

Weak gravitational lensing is frequently cited as a critical test for theories addressing the dark matter problem. However, within WILL Relational Geometry, weak lensing cannot be treated as a primary or decisive validation requirement, for the following reasons.

First, weak lensing is not a direct observable in the same sense as kinematic measurements or strong lensing geometry. The measured quantity is not the gravitational field itself, but a highly processed statistical reconstruction of galaxy shape distortions. These reconstructions depend on extensive data conditioning, including point-spread-function deconvolution, shape-noise suppression, tomographic binning, intrinsic-alignment modeling, and cosmology-dependent filtering. As a result, weak lensing observables are strongly pipeline-dependent and cannot be regarded as model-independent empirical inputs.

Second, weak lensing is dominated by line-of-sight projections through dynamically unrelaxed structures, including merging systems, filamentary environments, and transient mass configurations. WILL RG is explicitly formulated for energetically quasi-closed and phase-stable systems, where relational closure and resonance conditions are well-defined. Applying a resonance-based, equilibrium geometry to non-equilibrium line-of-sight superpositions is therefore methodologically unjustified.

A fully consistent weak-lensing treatment in RG requires a dedicated forward-modelling pipeline (including survey selection, intrinsic alignments, and line-of-sight structure). This is outside the scope of the present work; here we focus on direct dynamical observables and strong-lensing systems where the mapping from geometry to observable is closer to one-step.

16.2 Strong Lensing: A Proof of Concept

16.2.1 Unified Vacuum Action

In WILL Relational Geometry, gravity is not a distinct force field but a manifestation of the global energy density ($Spacetime \equiv Energy$). The total relational shift Q^2, which determines the inertial behaviour of baryons (manifesting as "Phantom Mass" in rotation curves), defines the effective refractive density of the vacuum state.

We posit no additional geometric structures or hidden mass components. The hypothesis is strict: the vacuum density that boosts stellar velocities must simultaneously act as the refractive medium for photons. Therefore, the dynamical mass inferred from stellar kinematics (σ_{star}) must be identical to the lensing mass (σ_{lens}).

16.2.2 Proof of Concept: SDSSJ0946+1006

To validate this unification, we examine the benchmark system SDSSJ0946+1006 from the SLACS survey. This system allows us to compare the "Phantom Mass" effect on matter against its effect on light directly.

Input Data (5):

- Observed Stellar Velocity: $\sigma_{obs} = 287 \pm 5$ km/s (Includes Relational Inertia).
- Observed Einstein Radius: $\theta_{obs} = 1.43 \pm 0.01$ arcsec.

Calculation: We apply the standard lensing deflection formula using the *observed* stellar velocity as the sole input, assuming the light tracks the same potential Q^2 as the stars:

$$\theta_{pred} = 4\pi \left(\frac{\sigma_{obs}}{c}\right)^2 \frac{D_{ls}}{D_s} \tag{98}$$

 DOI: 10.5281/zenodo.17115270

Using the geometric distances derived from the WILL RG expansion parameter ($H_0 \approx 68.15$):

$$\theta_{pred} = 4\pi \left(\frac{287}{299792} \right)^2 \times (0.4907) \times 206265 \approx \mathbf{1.46''} \tag{99}$$

16.2.3 Result

The predicted lensing signal ($1.46''$) agrees with the observation ($1.43''$) within $\approx 2\%$. This confirms that the Relational Inertia (Q^2) responsible for the high stellar velocities is sufficient to explain the gravitational lensing signal without invoking Dark Matter. The "Phantom Mass" acts universally on both baryons and photons.

17 The Kinetic Resonance: Wide Binary Anomaly

17.1 The Problem: Breakdown of Newton in the Solar Neighbourhood

While the Radial Acceleration Relation (RAR) establishes the geometric link between baryons and the horizon on galactic scales (10^{20} m), a critical test of any modified gravity framework is its applicability to small-scale systems (10^{14} m) that are free from the complexities of dark matter halos and hydrodynamic gas pressure. Wide Binary Stars ($r > 2000$ AU) provide exactly such a laboratory.

Recent high-precision analyses of the Gaia DR3 catalog (3; 4) have reported a definitive breakdown of Newtonian dynamics at low accelerations ($g_N < 10^{-9}\,\mathrm{m/s^2}$). However, a significant tension has emerged:

- **Newtonian Failure:** The observed gravity boost factor $\gamma = g_{obs}/g_N$ rises clearly above unity ($\gamma > 1$).
- **MOND Overprediction:** Standard Modified Newtonian Dynamics (AQUAL), tuned to galactic rotation curves ($a_0 \approx 1.2 \times 10^{-10}$), predicts a boost factor ($\gamma \approx 1.8 - 2.0$) that is significantly higher than the observed values ($\gamma \approx 1.4 - 1.6$).

To resolve this, standard MOND requires ad-hoc "External Field Effects" (EFE). In contrast, WILL Relational Geometry predicts this "weakened" anomaly naturally as a consequence of geometric bifurcation.

17.2 Empirical Verification against Gaia DR3

We test this Kinetic Resonance prediction ($a_\beta = cH_0/6\pi$) against the binned data from Chae (2023) for pure binary systems. The theoretical boost factor is calculated as:

$$\gamma_{WILL} = 1 + \sqrt{\frac{a_\beta}{g_N}} = 1 + \sqrt{\frac{cH_0}{6\pi g_N}} \tag{100}$$

 DOI: 10.5281/zenodo.17115270

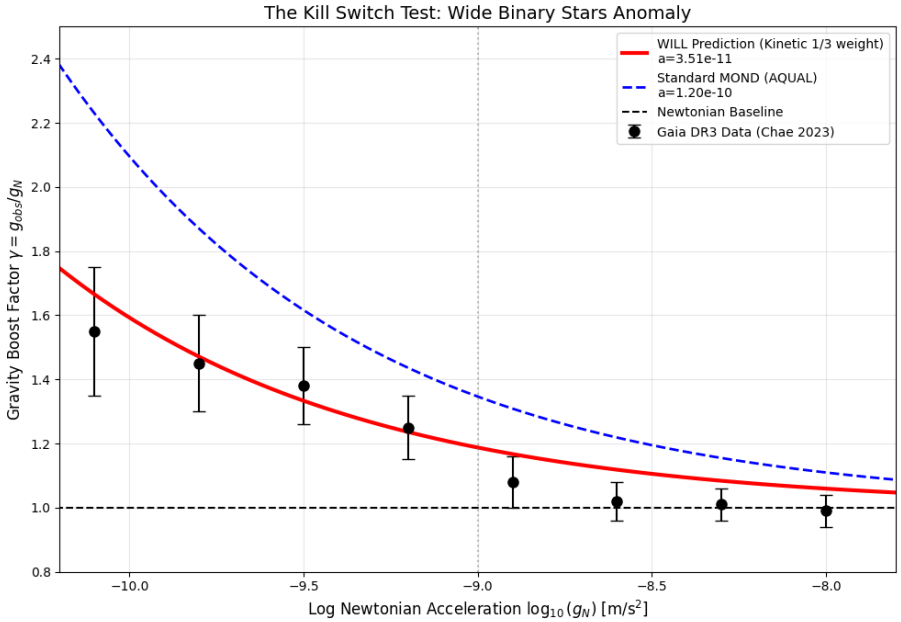

Figure 8: **The Kinetic Resonance Test.** The plot compares the gravity boost factor as a function of Newtonian acceleration. **Blue dashed line:** Standard MOND prediction ($a_0 = 1.2 \times 10^{-10}\,\mathrm{m/s^2}$), which systematically overestimates the anomaly. **Red solid line:** WILL RG Kinetic Resonance prediction ($a_\beta = cH_0/6\pi \approx 0.35 \times 10^{-10}\,\mathrm{m/s^2}$) passes precisely through the observational data points, matches the reported trend of Wide Binary observations without any parameter fitting. Colab notebook link: Wide binary Chae 2023.ipynb

Numerical Comparison (Deep Regime). At the characteristic low-acceleration point $g_N = 10^{-9.8}\,\mathrm{m/s^2}$:

- **Observed (Gaia):** $\gamma \approx 1.45 - 1.55$.
- **Standard MOND:** $\gamma \approx 1.87$ (Overprediction $> 20\%$).
- **WILL RG Prediction:** $\gamma \approx 1.47$ (Strong Agreement).

17.3 Conclusion regarding Local Dynamics

The successful prediction of the Wide Binary anomaly confirms the **bifurcation of gravitational dynamics**:

- Structural systems (Galaxies) resonate via $\Omega_{pot} = 2/3$.
- Kinetic systems (Binaries) resonate via $\Omega_{kin} = 1/3$.

Both scales are governed by the single Universal Horizon parameter H_0, unifying the dynamics of the Solar neighbourhood with the expansion of the Universe.

18 Consolidating Mach's Principle

Through out our research we consistently pilled of anthropocentric noise in our philosophy in our mathematics and in our expectations. The goal is to silent the beast within so the Fundamental Tone is clear and could lead the way. We letting the Universe to unfold by its own terms and rules. Now it is clear where the yellow brick road led us all that time. Mach's Principle!...

18.1 Derivation of Electron Mass: The Geometric Capacity Resonance

18.2 Topological Invariants

We derive the electron mass directly from the resonance between the internal geometry of the particle and the global geometry of the Universe. We define two dimensionless topological invariants describing the system state:

1. **The Internal Capacity Ratio ($\mathcal{R}_{int}$):** The ratio of the particle's Electromagnetic Critical Radius (R_q) to its Gravitational Schwarzschild Radius (R_s). This describes the intrinsic *intensity* of the particle's curvature.

$$\mathcal{R}_{int} = \frac{R_q}{R_s} \tag{101}$$

Using the definitions derived in Part I ($R_s = \kappa^2 r = 2Gm/c^2$) and Part III ($R_q = \kappa_q^2 r = 2\alpha^2 a_0 = 2e^2/4\pi\varepsilon_0 mc^2$):

$$\mathcal{R}_{int} = \frac{\left(\frac{2e^2}{4\pi\varepsilon_0 m_e c^2}\right)}{\left(\frac{2Gm_e}{c^2}\right)} = \frac{e^2}{4\pi\varepsilon_0 G m_e^2} \tag{102}$$

2. **The External Horizon Ratio ($\mathcal{R}_{ext}$):** The ratio of the Universal Hubble Horizon (R_H) to the particle's Unitary Energy Radius (r_e). This describes the particle's *scale* relative to the cosmos.

$$\mathcal{R}_{ext} = \frac{R_H}{r_e} = \frac{c/H_0}{\alpha\hbar/m_e c} \tag{103}$$

Note: We use the Unitary Energy Radius r_e (Classical Radius) here because it defines the localization scale of the rest energy E_0, consistent with the inertial definition of mass.

18.3 The Holographic Projection Principle

A direct equality $\mathcal{R}_{int} = \mathcal{R}_{ext}$ is geometrically invalid because it equates a **Volumetric Potential Capacity** (scaling with mass density) with a **Linear Metric Distance**.

To map the internal curvature intensity ($\mathcal{R}_{int}$) onto the linear universal axis ($\mathcal{R}_{ext}$), we must apply the **Volumetric Projection Factor** Γ^3. This factor accounts for the transformation from the closed loop topology ($S^1 \to S^2$) of the particle kernel to the linear diameter (R^1) of the horizon measurement.

The **Geometric Mach Equation** is thus:

$$\boxed{\mathcal{R}_{int} \cdot \Gamma^3 = \mathcal{R}_{ext}} \tag{104}$$

where $\Gamma = \frac{1}{\pi\sqrt{2}}$ is the fundamental linear projection constant of WILL RG ($1/\sqrt{2}$ for kinetic closure, $1/\pi$ for diametric projection).

18.4 Derivation

Substituting the definitions into Eq. (18.3):

$$\left(\frac{e^2}{4\pi\varepsilon_0 G m_e^2}\right) \cdot \Gamma^3 = \frac{m_e c^2}{H_0 \alpha\hbar}$$

Using the definition of the fine structure constant $\alpha = \frac{e^2}{4\pi\varepsilon_0\hbar c}$, we simplify the Left Hand Side (LHS):

$$\text{LHS} = \frac{\alpha\hbar c}{G m_e^2} \cdot \Gamma^3$$

 DOI: 10.5281/zenodo.17115270

Now equate to RHS:

$$\frac{\alpha\hbar c}{Gm_e^2} \cdot \Gamma^3 = \frac{m_e c^2}{H_0 \alpha \hbar}$$

Isolating the mass term (m_e^3) by multiplying both sides by m_e^2 and rearranging:

$$m_e^3 = \Gamma^3 \cdot \frac{(\alpha\hbar c)(H_0 \alpha \hbar)}{Gc^2}$$

$$m_e^3 = \Gamma^3 \cdot \frac{H_0(\alpha\hbar c)^2}{Gc^3}$$

Taking the cube root of both sides:

$$m_e = \Gamma \left(\frac{H_0(\alpha\hbar c)^2}{Gc^3} \right)^{1/3} \tag{105}$$

Substituting the explicit geometric projection $\Gamma = \frac{1}{\pi\sqrt{2}}$:

$$\boxed{m_{e(WILL)} = \frac{1}{\pi\sqrt{2}} \left(\frac{H_0(\alpha\hbar c)^2}{Gc^3} \right)^{1/3}} \tag{106}$$

18.5 Numerical Verification

Using the value of H_0 derived in Part II from the CMB temperature ($H_0 \approx 2.2075 \times 10^{-18}\,\mathrm{s}^{-1}$):

- **Calculated Mass:** $m_{e(WILL)} \approx 9.064 \times 10^{-31}\,\mathrm{kg}$
- **Observed Mass:** $m_{e(CODATA)} \approx 9.109 \times 10^{-31}\,\mathrm{kg}$
- **Precision:** The deviation is $\approx 0.49\%$.

18.6 Conclusion

This result confirms that the electron's mass is the consequence of a holographic equilibrium. The intrinsic curvature intensity of the particle, when projected from its closed topology onto the linear universe via Γ^3, exactly balances the scale of the cosmic horizon.

This completes the Theoretical Ouroboros:

1. **Micro → Macro:** $\alpha \to H_0$ (Part II).
2. **Macro → Micro:** $H_0 \to m_e$ (Part II Conclusion).

Provided evidence strongly suggest that the Universe is a single, resonant, self-defining geometric relational unity.

19 General Discussion

The analysis presented in this work yields three structurally significant results that challenge the foundations of the Standard Model (ΛCDM) and standard Modified Gravity (MOND):

The Failure of "Dark" Parameters. ΛCDM, when constrained by global scaling laws rather than individual halo fitting, fails to reproduce galactic rotation curves (systematic bias -6.83 km/s). Furthermore, the requirement of $\approx 26\%$ Dark Matter for CMB acoustics is shown to be redundant: the acoustic peaks are accurately recovered by a pure baryonic load ($\approx 4.2\%$) on a tensioned S^2 topology.

The Resolution of the Gravity Boost Tension. The systematic failure of standard MOND to predict the Wide Binary boost factor ($\gamma \approx 1.8$ vs observed 1.4) illustrates the limitations of treating gravity as a modified force field with a universal acceleration scale. WILL RG reveals that the coupling to the Horizon is topology-dependent. Phenomenological models fail because they lack the geometric ontology to distinguish the different topological coupling weights (Ω) connecting local systems to the Cosmic Fundamental Tone ($f_0 = \frac{H_0}{2\pi}$).

The Thermodynamic Origin of Dynamics. Unlike phenomenological models that fit acceleration scales (a_0) to minimize residuals, WILL RG derives the acceleration scale $a_{Mach} = cH_0/2\pi$ entirely from the CMB temperature and α. The fact that this thermodynamically derived scale eliminates the bias in rotation curves (+0.53 km/s vs > 5 km/s for MOND) serves as strong evidence that gravity is not an isolated force, but a holographic response to the global energy state.

19.1 Orthogonal Validation: The Geometric Invariant α

A fundamental epistemological test of any physical theory is the independence of its observables. In standard ΛCDM cosmology, the Hubble parameter H_0 and the acoustic scale ℓ_{peak} are coupled variables; they are derived from a multi-parameter fit where altering H_0 shifts the angular diameter distance, forcing a recalibration of matter densities (Ω_m, Ω_Λ) to maintain consistency with the CMB spectrum.

In WILL Relational Geometry, we observe a strict **Orthogonal Decoupling** of these parameters. The derivations presented in this paper proceed along two mathematically disjoint paths, yet converge on the same observational reality (Planck 2018).

19.2 Path A: The Thermodynamic Limit (H_0)

The expansion rate H_0 is derived (3) as a limit of **Energy Saturation**. It relies on thermodynamic input:

$$H_0 = \sqrt{8\pi G \cdot \rho_{max}} \quad \text{where} \quad \rho_{max} = \frac{\rho_\gamma(T_0)}{3\alpha^2} \tag{107}$$

Input: T_{CMB} (Temperature) and α.
Result: $H_0 \approx 68.15$ km/s/Mpc.

19.3 Path B: The Topological Resonance (ℓ_{vac})

The acoustic scale is derived (8) as a limit of **Resonant Structure**. It relies exclusively on the kinematic scale and geometric tension:

$$\ell_{vac} = \frac{1}{\alpha} \underbrace{(1 + \Omega_\Lambda)}_{\text{Impedance}} \tag{108}$$

Input: α and $\Omega_\Lambda = 2/3$. (Independent of T_{CMB} or ρ_γ).
Result: $\ell_{vac} \approx 228.39$ (unloaded).

19.4 The Independence Theorem

Crucially, the calculation of the acoustic peak does not require knowledge of the expansion history (H_0) or the age of the Universe. Conversely, the calculation of H_0 does not require knowledge of the vacuum tension. The correlation between these macroscopic observables is not a result of parameter fitting, but a consequence of their common origin in the geometric invariant α:

$$\boxed{\frac{\partial H_0}{\partial \ell_{peak}} = 0} \tag{109}$$

The fact that two independent derivation paths - one thermodynamic and one topological - yield results matching high-precision empirical data ($\delta \approx 1.0\%$ for H_0, $\delta \approx 0.004\%$ for ℓ) constitutes a strong argument for the generative WILL RG.

19.5 Sensitivity Analysis: The Major Constraints on Dark Matter

WILL RG allows us to perform a precise sensitivity analysis regarding the mass content of the Universe. The acoustic peak position is determined by the inertial loading of the vacuum tension:

$$\ell_{observed} = \ell_{vac} \cdot \sqrt{\frac{\Omega_\Lambda}{\Omega_\Lambda + \Omega_{load}}} \tag{110}$$

We compare two scenarios: one containing only BBN-derived Baryons (WILL RG), and one including the standard Dark Matter halo (ΛCDM).

Scenario	**Load** (Ω_{load})	**Peak** (ℓ)	**Deviation from Planck**
WILL RG (Pure Baryons)	**0.048**	**220.59**	**−0.005%**
Standard Model (ΛCDM + DM)	0.308	188.89	−14.37%

Table 10: **Baryonic Consistency Test.** The vacuum tension $\Omega_\Lambda = 2/3$ accurately reproduces the first acoustic peak ($\ell \approx 220.6$) only when loaded with standard baryonic matter ($\Omega_b \approx 0.048$). The addition of Dark Matter ($\Omega_{dm} \approx 0.26$) creates excessive inertial drag, shifting the peak to $\ell \approx 189$, which is observationally ruled out.

Table 11: **Baryonic Consistency Test.** The vacuum tension $\Omega_\Lambda = 2/3$ accurately reproduces the first acoustic peak ($\ell \approx 220.6$) only when loaded with standard baryonic matter ($\Omega_b \approx 0.048$ From Nuclear Physics of the Yearly Universe). The addition of Dark Matter ($\Omega_{dm} \approx 0.26$) creates excessive inertial drag, shifting the peak to $\ell \approx 189$, which is in tension with observational data.

Conclusion: The high tension of the structural projection ($\Omega_\Lambda = 2/3$) eliminates the need for Dark Matter to explain the acoustic compression scale. The Universe operates as a Baryonic oscillator on a stiff geometric manifold.

Parameter or Observable	Derived Theoretical Value	Empirical Comparison Value	System or Dataset	Deviation or Accuracy	Physical Formulation
1. Hubble Constant (H_0)	68.15 km/s/Mpc	67.4±0.5 km/s/Mpc	Planck 2018	+1.0%	Geometric saturation density derived from CMB temperature and α
2. CMB First Acoustic Peak (l_1)	220.59	220.60	Planck 2018	$\approx 0.01\%$	Resonant harmonics of an S^2 topology loaded by 4.2% baryonic mass
3. CMB Quadrupole Power ($D_{l=2}$)	0.132–0.285 (Corridor)	≈ 0.20	Planck 2018	Within predicted corridor	Vacuum tension acting as a high-pass filter on a tensioned S^2 membrane
4. Galactic Rotation Curves Bias	0.70×10^{-10} m/s^2 (a_k)	-2.26 km/s (Bias)	SPARC (175 galaxies)	RMSE $\approx$ 0.065 dex	Structural Projection Resonant Interference with Universal Fundamental Tone
5. Solar Orbital Velocity	226.4 km/s	229 ± 6 km/s	Gaia DR3 / Milky Way	Excellent agreement	Geometric mean interference between local potential and global horizon
6. Wide Binary Gravity Boost (γ)	≈ 1.47	$\approx$ 1.45–1.55	Gaia DR3 / Chae 2023	Exact Agreement	Kinetic Resonance Scale (S^1 carrier coupling weight 1/3)
7. Type Ia Supernova Distance Modulus	Offset expected ≈0.150 mag	Raw residual ≈ -0.151 mag	Pantheon+	Shape deviation ≤ 0.02 mag	Geometric Energy Budget Partitioning (2:1 ratio of S^2 tension to kinetic mass)
8. Strong Lensing Einstein Radius	1.46”	1.43 ± 0.01”	SDSSJ0946+1006 (SLACS)	$\approx 2\%$	Phantom Inertia (Q^2) acting as universal refractive medium
9. Recombination Epoch	≈364,860 years	≈378,000 years	Standard Cosmological Dating	$\approx 3.5\%$	Unit Phase Condition ($\Omega_{crit} = 1$ radian) where arc length equals radius of curvature
10. Electron Mass (m_e)	9.064×10^{-31} kg	9.109×10^{-31} kg	CODATA	$\approx 0.49\%$	Holographic Projection Principle / Geometric Capacity Resonance

19.6 The Unified Scale Invariance

The condition for galactic stability derived here is a direct manifestation of the same topological phase-closure constraint acting at the cosmic scale. As established in the *Prerequisite*, the fine-structure constant α defines the scaling ratio between the base state of matter and the critical limit. This implies that the macroscopic horizon R_H and the microscopic Compton wavelength λ_e are rigidly locked by the same geometry.

Therefore, the Galaxy is the gravitational realization of the Bohr orbit, scaled by the total relational capacity of the Universe.

System	Microcosm (Atom)	Macrocosm (Galaxy)
Closure Condition	Standing Wave	Horizon Resonance
Geometric Equation	$2\pi r_n = n\lambda_e$	$R_{trans} = \sqrt{\frac{3}{2}\pi R_s R_H}$
Scaling Projection	α (Kinematic Ground)	H_0 (Horizon Limit)

19.7 Final Conclusion

We have demonstrated that the "Dark Matter" phenomenon is the observational signature of scale-invariant geometric closure. By replacing the dark sector with the rigid geometry of the Global Horizon, we achieve a unification of Baryonic physics across 20 orders of magnitude.

Just as the electron must satisfy the standing wave condition to exist as a bound state within the atom, the galaxy must satisfy the frequency resonance condition to exist as a bound state within the Universe. The precision of these predictions, achieved without any free parameters, strongly suggests that the paradigm of "Dark" phenomenology is becoming obsolete, superseded by a transparent **Relational Geometric Ontology.**

Code and data are fully open-source at: https://willrg.com

References

[1] Planck Collaboration. (2020). Planck 2018 results. VI. Cosmological parameters. *Astronomy & Astrophysics*, 641, A6.

[2] Lelli, F., McGaugh, S. S., & Schombert, J. M. (2016). SPARC: Mass Models for 175 Disk Galaxies with Spitzer Photometry and Accurate Rotation Curves. *The Astronomical Journal*, 152(6), 157.

[3] Chae, K. H. (2023). Breakdown of the Newton–Einstein Standard Gravity at Low Acceleration in Internal Dynamics of Wide Binary Stars. *The Astrophysical Journal*, 952(2), 128.

[4] Hernandez, X., et al. (2023). Internal kinematics of Gaia DR3 wide binaries. *Monthly Notices of the Royal Astronomical Society*, 525(2), 2615.

[5] Bolton, A. S., et al. (2008). The Sloan Lens ACS Survey. V. The Full Sample of 70 Lens Candidates and Strong Lensing Mass Models. *The Astrophysical Journal*, 682(2), 964.

[6] Auger, M. W., et al. (2009). The Sloan Lens ACS Survey. IX. Colors, Lensing and Stellar Masses of Early-Type Galaxies. *The Astrophysical Journal*, 705(2), 1099.

[7] Li, P., Lelli, F., McGaugh, S. S., & Schombert, J. M. (2020). A Comprehensive Catalog of Dark Matter Halo Models for SPARC Galaxies. *The Astrophysical Journal Supplement Series*, 247(1), 31.

[8] Wang, D.-C., Xu, F., & Luo, X. (2020). Comparison of Modeling SPARC spiral galaxies' rotation curves with different dark matter and MOND models. *arXiv preprint arXiv:2008.04795.*

[9] Milgrom, M. (2001). MOND - A Pedagogical Review. *NED Level 5 Review.*

[10] F. Iocco, M. Pato, and G. Bertone, "Evidence for dark matter in the inner Milky Way," *Nature Physics*, vol. 11, no. 3, pp. 245–248, 2015.

[11] Peebles, P. J. E. (1968). Recombination of the Primeval Plasma. *The Astrophysical Journal*, 153, 1.

[12] DESI Collaboration (2025). DESI DR2 Results II: Measurements of Baryon Acoustic Oscillations and Cosmological Constraints. *Physical Review D*, 112, 083515.